sustainability

MDPI

Article

An Improved Differential Evolution for Parameter Identification of Photovoltaic Models

Shufu Yuan [1], Yuzhang Ji [1], Yongxu Chen [1], Xin Liu [1] and Weijun Zhang [1,2,*]

[1] School of Metallurgy, Northeastern University, Shenyang 110819, China; 2101596@stu.neu.edu.cn (S.Y.)
[2] State Environmental Protection Key Laboratory of Eco-Industry, Northeastern University, Shenyang 110819, China
* Correspondence: zhangweijun@smm.neu.edu.cn

Abstract: Photovoltaic (PV) systems are crucial for converting solar energy into electricity. Optimization, control, and simulation for PV systems are important for effectively harnessing solar energy. The exactitude of associated model parameters is an important influencing factor in the performance of PV systems. However, PV model parameter extraction is challenging due to parameter variability resulting from the change in different environmental conditions and equipment factors. Existing parameter identification approaches usually struggle to calculate precise solutions. For this reason, this paper presents an improved differential evolution algorithm, which integrates a collaboration mechanism of dual mutation strategies and an orientation guidance mechanism, called DODE. This collaboration mechanism adaptively assigns mutation strategies to different individuals at different stages to balance exploration and exploitation capabilities. Moreover, an orientation guidance mechanism is proposed to use the information of the movement direction of the population centroid to guide the evolution of elite individuals, preventing them from being trapped in local optima and guiding the population towards a local search. To assess the effectiveness of DODE, comparison experiments were conducted on six different PV models, i.e., the single, double, and triple diode models, and three other commercial PV modules, against ten other excellent meta-heuristic algorithms. For these models, the proposed DODE outperformed other algorithms, with the separate optimal root mean square error values of $9.86021877891317 \times 10^{-4}$, $9.82484851784979 \times 10^{-4}$, $9.82484851784993 \times 10^{-4}$, $2.42507486809489 \times 10^{-3}$, $1.72981370994064 \times 10^{-3}$, and $1.66006031250846 \times 10^{-2}$. Additionally, results obtained from statistical analysis confirm the remarkable competitive superiorities of DODE on convergence rate, stability, and reliability compared with other methods for PV model parameter identification.

Keywords: photovoltaic models; parameter identification; differential evolution; mutation strategy; orientation guidance

Citation: Yuan, S.; Ji, Y.; Chen, Y.; Liu, X.; Zhang, W. An Improved Differential Evolution for Parameter Identification of Photovoltaic Models. *Sustainability* **2023**, *15*, 13916. https://doi.org/10.3390/su151813916

Academic Editor: Cristina Ventura

Received: 8 August 2023
Revised: 2 September 2023
Accepted: 15 September 2023
Published: 19 September 2023

1. Introduction

With the progress of human society, the depleted stocks of fossil energy cannot meet the increasing energy requirement. Moreover, the applications of fossil energy have resulted in a series of environmental deterioration issues, including air pollution and the greenhouse effect [1–3]. Therefore, the development and utilization of clean energy, such as solar, biomass, hydrogen, wind, water, and nuclear energy, will help alleviate the present energy crisis. Recently, the attention paid to solar energy, among numerous clean energy sources, has sharply increased because of its wide distribution and easy availability [4]. In the electric power industry, photovoltaic (PV) generation systems enable the conversion of solar energy into electricity, where this transformation is implemented by solar cells. However, solar panels are susceptible to adverse weather conditions and environmental factors due to their year-round outdoor operation, including the shortening of the service life of solar cells and reduction in the output of power and energy conversion efficiency [5,6]. To achieve

maximized and steady conversion efficiency for PV systems in diverse environments and complex scenarios, it becomes imperative to find a feasible method for accurately simulating, optimizing, and controlling corresponding PV models.

By constructing the mathematical representation of the PV generation system, significant progress has been achieved in recent years in understanding the operation function of PV systems [7]. The bulk of models aim to realize the optimal fit to the actual measurement of current–voltage data obtained from PV cells [8]. Most research focuses on constructing equivalent circuits with diodes to simulate the real behavior of PV cells due to the similarity between the output characteristics of the p-n junction of a diode and a PV cell [9]. Among various PV models, the single diode model (SDM), double diode model (DDM), triple diode model (TDM), and PV module models have been applied extensively in practice [10]. It is noteworthy that the dynamic behavior of these models depends on several unknown parameters, including photocurrent, diode saturation current and ideal factor, and shunt and series resistances. Additionally, these parameters are easily influenced by complex factors, such as device aging, malfunctions, and volatile operations. Thus, the accurate identification of these unknown parameters associated with PV models is an arduous but meaningful task for augmenting the performance of solar generation systems.

In recent years, numerous mature techniques have been presented and used in the parameter identification of PV models [11,12]. There are mainstream techniques, including analytical, iterative-based methods and meta-heuristic algorithms (MHAs) [13]. The analytical method employs a series of mathematical formulas to identify model parameters. Although this method is implemented readily, it is highly dependent on the initial conditions and normally has a high computational cost. Accordingly, it is not efficient in solving the parameter identification of PV models with multi-modal and non-linear features [14]. The second method, i.e., the iterative-based method, mainly comprises the Lambert W functions [15] and Newton–Raphson [16] methods, which are easily trapped in local optima of multi-modal functions due to excessive reliance on initial values and the gradient information of the problem [17]. Fortunately, MHAs have surmounted these limitations since this algorithm remains unaffected by initial conditions and does not depend on the problem features [18,19]. MHAs also achieve high solution accuracy and competitive computational efficiency compared to traditional methods when tackling complex problems [20]. Representative approaches are differential evolution (DE) [21,22], particle swarm optimization (PSO) [23,24], gaining-sharing knowledge algorithm (GSK) [20,25], whale optimization algorithm (WOA) [26,27], genetic algorithm (GA) [28], artificial bee colony optimization (ABC) [29,30], Grey-wolf optimization [31], and JAYA optimization [32,33], among many advanced algorithms [34–38]. Many MHAs have obtained excellent performances for the parameter estimation of PV models. Actually, researchers are inclined to use modified versions of algorithms due to the finite performance of the originals when estimating parameters of PV models. A differential evolution using a novel penalty method (P-DE) was developed for the parameter identification of some multi-crystalline, mono-crystalline, and thin-film modules [22]. Gao et al. [21] presented a directional permutation DE (DPDE) to determine parameters in the SDM, DDM, TDM, and three other PV module models. The compared experiment results demonstrated its higher solving accuracy than that of other optimization algorithms. Recently, Gu et al. [39] introduced an elite learning adaptive DE variant (ELADE) with a parameter adaptive strategy and an elite mutation strategy applied to obtain the characteristics of several PV models. Jordehi et al. [40] developed a modified time-varying PSO algorithm by controlling the individual acceleration coefficients (TVACPSO) to achieve a trade-off for exploration and exploitation to accurately estimate the photovoltaic model parameters. Given the complex features of PV representations, a PSO variant incorporating a mutation idea from DE was employed to mitigate premature convergence for parameter estimation of the SDM, DDM, poly-crystalline Photo Watt-PWP 201, and multi-crystalline IFRI250-60 modules [41]. A dual-population GSK algorithm (DPGSK) was developed for accurate parameter identification in PV system modeling [42]. DPGSK employs a dual-population evolution strategy to balance exploration and exploita-

tion to improve the convergence rate and population diversity. The results confirm that the parameter extraction accuracy of DPGSK outperforms that of the other methods. An improvement of GA, incorporating a novel convex crossover method, was presented to balance the population diversification and solution accuracy of GA [43]. Afterward, a GA adopting non-uniform mutation and blend crossover operators (GAMNU) was constructed for the parameter extraction of two simple PV models and three other commercial solar cells [44]. Chen et al. [29] proposed an ABC algorithm combined with teaching–learning-based optimization (TLABC) to be employed for the parametric extraction of three common PV models. In [45], an improved artificial bee colony optimization algorithm based on the chaotic map theory (CIABC) was developed to fortify the search capability of ABC at PV parameter extraction. In [46], a hunter–prey optimization algorithm with reciprocity and sharing and learning interaction was presented to identify the unknown parameters of several PV models. Furthermore, Sharma et al. [47] proposed an improved moth flame optimization technique with the opposite learning method and Lévy flight mechanism (OBLVMFO) to identify parameters of three PV panels, i.e., the STE 4/100 and SS2018P poly-crystalline, and LSM20 mono-crystalline modules. In addition to improving parameter identification accuracy, from a non-parametric statistical perspective, OBLVMFO exhibits significantly better optimization performance than the classical MFO. In [48], eight optimization techniques were applied in the parametric extraction of the R.T.C. France PV cells, and the LSM20 and SS2018 PV modules. The relevant experimental results assessed the capabilities of each improved algorithm in constructing PV models, thereby enhancing energy conversion efficiency. Due to space limitations, research on applying more MHAs to resolve the parameter identification problem in PV models can be found in [11,12,49,50].

Among numerous MHAs, the DE algorithm, judged one of the most effective optimization methods, has been employed widely for the parameter identification of various PV models and performs considerably well [21,51]. Relative research has mainly focused on the equilibrium between the exploration and exploitation capabilities of DE. For example, a differential evolution using self-adaptive multiple mutation strategies of the random assignment method (SEDE) was proposed for individuals based on the iterative process [52]. Afterward, an improved DE with one elite and obsolete dynamic learning, called DOLDE, used a dynamic oppositional learning mechanism to balance the global and local search abilities of individuals [53]. However, one easily overlooked fact is that the algorithmic exploration and exploitation capabilities should be determined comprehensively based on both the iteration process and the search inclinations of individuals. In the early stages, it is reasonable that the entire population conducts a global search, while the population should shift towards a local search in the later iterations. Each individual should be assigned different search tasks based on their fitness values at different stages. Considering the complex characteristics of the nonlinear, multivariate, and non-convex nature of parameter identification for photovoltaic models, the single mutation strategy often causes the DE algorithm to become trapped in a local optima, thereby losing its optimization capabilities. Furthermore, individuals with better fitness should focus on a local search due to the finite computational source, while those with relatively poor fitness should execute a global search. These elites should be allocated more computational resources, thereby guiding the population evolution.

Based on the above discussion, this paper designs a modified differential evolution with a collaboration mechanism of dual mutation strategies and an orientation guidance mechanism (DODE) for the accurate parameter identification of photovoltaic models. Specifically, a collaboration mechanism of dual mutation strategies is developed to coordinate the search tendencies of each individual in the population and make a trade-off between the exploration and exploitation capabilities of DE. Moreover, considering the complex feature of the parameter identification problem of the PV model, it is also crucial to rationally allocate computational resources. Some elites with better fitness values should be allocated more computational resources. However, for DE, elites have single evolutionary directions and are easily stuck at local optima. To address this issue, an orientation

guidance mechanism based on the population evolution trend is also developed to facilitate the evolution of elites, thereby effectively alleviating the state of elites being trapped in local optima.

The main contributions of this paper are as follows:

- An improved differential evolution is proposed by incorporating a collaboration mechanism of dual mutation strategies and an orientation guidance mechanism into it. The proposed DODE algorithm can accurately estimate many PV models' parameters due to its improved optimization ability.
- Extensive comparisons with ten advanced algorithms, including five improved DE algorithms and five other representative meta-heuristic algorithms, are conducted in six different PV models, i.e., the single diode, double diode, triple diode models, and Photowatt-PWP201, mono-crystalline STM6-40/36, and poly-crystalline STP6-120/36 module models.
- Experimental results show that the proposed DODE possesses the higher accuracy of parameter estimation by obtaining the minimum root mean square errors on these PV models.
- The convergence curves on the six PV models indicate that the proposed DODE provides the faster convergence speed. Statistical analyses also verify the significant competitive superiorities of DODE compared to other optimization algorithms.
- The proposed DODE algorithm yields a high exactitude in identifying parameters of PV models, with high similarity between the simulated data obtained by DODE and the experimentally measured data.

The structure of the remainder of this paper is arranged as follows: Section 2 elaborates on the problem of parameter estimation of the common PV models and formulates mathematical expressions. The classical DE algorithm and its principles are introduced in Section 3. Section 4 describes the proposed DODE algorithm for the parameter identification of PV models. The experiment results and statistical analyses are presented in Section 5. Finally, Section 6 summarizes the sections above while outlining future research directions.

2. Mathematical Modeling and Problem Formulation

In the literature [11,12,49,50], a series of mathematical expressions have been raised to explain the output characteristics of PV cells and modules, where the diode-based model is extensively employed. The reason for utilizing diode modeling in the equivalent circuit of PV cells is that the PV generation unit comprises semiconductors with an exponential current–voltage curve (*I*-*V*), the same as for the diode output characteristic. Each diode-based model embodies several unknown parameters that should be precisely identified (in the equivalent circuit). Accurately estimating unknown parameters is vital for the operation of the photovoltaic system, as previous studies have suggested that the value of photovoltaic model parameters may vary over time resulting from the nonlinear property of photovoltaic cells and their aging.

2.1. Single Diode Model (SDM)

The SDM is extensively utilized because of its simplicity, and its equivalent circuit is illustrated in Figure 1. This mainly consists of the following subassemblies: (1) a photogenerated current source that hinges on the properties of the semiconductor material, change in irradiation intensity, and ambient temperature; (2) a diode paralleling with the current source contemplates the p-n junction's physical effects; (3) a series resistance (R_s) that represents the inner ohmic losses of the PV cell, including contact resistance between electrode surfaces and silicon, and electrode resistances and line resistance [54]; (4) a shunt resistor (R_{sh}) that indicates the leakage current in the semiconductor.

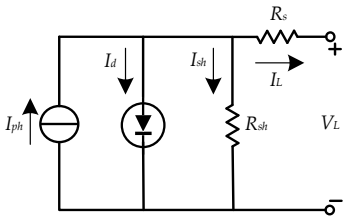

Figure 1. Equivalent circuit of SDM.

The combination of the diffusion and recombination currents of diodes and the determination of a non-physical factor for diode ideality are conducive to establishing the SDM [55]. Mathematically, the *I-V* characteristics of its equivalent circuit can be indicated as in Equation (1) [26].

$$I_L = I_{ph} - I_d - I_{sh} = I_{ph} - I_{sd}\left\{\exp\left[\frac{q(V_L + R_s I_L)}{nkT}\right] - 1\right\} - \frac{V_L + R_s I_L}{R_{sh}} \quad (1)$$

where I_L and V_L respectively express the measured current and voltage data from the PV cell. I_{ph} expresses the photogenerated current flowing through the p-n junction under irradiation, I_d indicates the diode current, I_{sh} indicates the shunt resistance current, I_{sd} represents the diode's reverse saturation current. R_s and R_{sh} respectively represent the values of the shunt and series resistors, n denotes the ideal factor of the diode, q is the charge of the electron (q = 1.6021766 × 10^{-19} C), k denotes the Boltzmann constant (k = 1.3806503 × 10^{-23} J/K), and T expresses the absolute temperature (Kelvin) of the PV cell. From Equation (1), it becomes evident that SDM contains five variables that must be exactly identified [I_{ph}, I_{sd}, R_s, R_{sh}, n]. Furthermore, in mathematical terms, "exp" represents the exponential function with the base of the natural constant e.

2.2. Double Diode Model (DDM)

Although the single diode model is mathematically valid for almost all types, its performance is not ideal when applied to thin films or underlying the low irradiation intensity. In practical applications, the current source will also be shunted through another diode to simulate the space-charge recombination current [56], and the partial short-circuit current route near the cell's periphery caused by semiconductor impurities and nonideality will be contemplated through the shunt leakage resistance. To handle this, the double diode model (DDM) is devised to regard the influence caused by the recombination current loss that emerged from the depletion region [57], as illustrated in Figure 2. The attraction is that its structure is not complicated and performs well under low irradiation. The following equation numerates the relevant output current [29]:

$$\begin{aligned} I_L &= I_{ph} - I_{d1} - I_{d2} - I_{sh} \\ &= I_{ph} - I_{sd1}\left\{\exp\left[\frac{q(V_L+R_s I_L)}{n_1 kT}\right] - 1\right\} - I_{sd2}\left\{\exp\left[\frac{q(V_L+R_s I_L)}{n_2 kT}\right] - 1\right\} - \frac{V_L+R_s I_L}{R_{sh}} \end{aligned} \quad (2)$$

where I_{sd1} and I_{sd2} respectively express the diode diffusion and saturation currents, and n_1 and n_2 are the ideal factors for the corresponding diodes. Accordingly, seven undetermined parameters of the DDM can be indicated by the row vector [I_{ph}, I_{sd1}, I_{sd2}, R_s, R_{sh}, n_1, n_2].

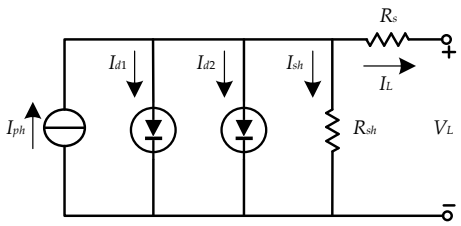

Figure 2. Equivalent circuit of DDM.

2.3. Triple Diode Model (TDM)

As shown in Figure 3, TDM incorporates three diodes to emulate the leakage current occurring in the grain boundaries of solar cells [58]. TDM expressly contains the various current components in solar cells and exhibits higher accuracy in fitting characteristic curves than SDM and DDM. However, it requires a substantial amount of time for execution and entails intricate hardware implementation. Therefore, TDM is best suited for replicating the *I-V* characteristics of large-scale industrial silicon solar cells [59]. Equation (3) is employed to express the output current within the framework of the associated equivalent circuit [60].

$$\begin{aligned} I_L &= I_{ph} - I_{d1} - I_{d2} - I_{d3} - I_{sh} \\ &= I_{ph} - I_{sd1}\left\{\exp\left[\frac{q(V_L+R_sI_L)}{n_1kT}\right]-1\right\} - I_{sd2}\left\{\exp\left[\frac{q(V_L+R_sI_L)}{n_2kT}\right]-1\right\} \\ &\quad -I_{sd3}\left\{\exp\left[\frac{q(V_L+R_sI_L)}{n_3kT}\right]-1\right\} - \frac{V_L+R_sI_L}{R_{sh}} \end{aligned} \tag{3}$$

where I_{sd3} and n_3 denote the newly added diode saturation current and the ideal factor, respectively. For this model, nine undetermined variables, including I_{ph}, I_{sd1}, I_{sd2}, I_{sd3}, R_s, R_{sh}, n_1, n_2, and n_3, need to be precisely identified.

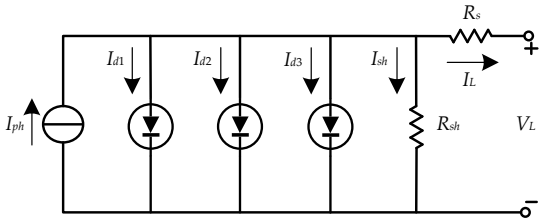

Figure 3. Equivalent circuit of TDM.

2.4. PV Module Model

Typically, the single PV cell's voltage magnitude and output power are considerably restricted and can no longer satisfy the actual demands. For this reason, the PV module model, comprising an arrangement of solar cells interconnected in series and parallel constructions, has been presented to overcome the single PV cell's lack of output power. Specifically, the solar cells are organized in a series of strings linked in parallel. Each cell string is serially connected to a blocking diode to mitigate the risk of excess current flowing back into a line during a cell failure. Furthermore, in a series grouping, a bypass diode is employed to shift the output current if one or more cells within the group fail or become blocked. A common PV module model based on the single diode is depicted in Figure 4, and its output current is numerated by Equation (4) [61].

$$I_L = I_{ph} - I_{sd}\left\{\exp\left[\frac{q(V_L/N_s + R_sI_L/N_p)}{nkT}\right]-1\right\} - \frac{V_L/N_s + R_sI_L/N_p}{R_{sh}} \tag{4}$$

where N_s and N_p respectively indicate the number of PV cells in series and parallel. Similar to SDM, the PV module model requires correctly identifying several previously undetermined parameters, i.e., I_{ph}, I_{sd}, R_s, R_{sh}, and n.

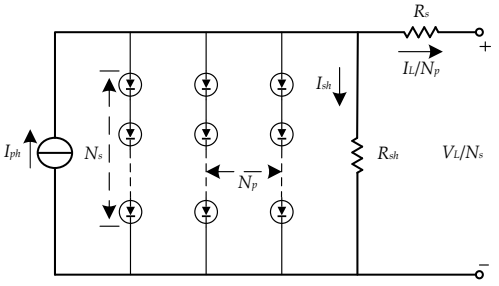

Figure 4. Equivalent circuit of PV module model.

2.5. Problem Formulation

The identification of unknown parameters of PV cells and module models can be easily summarized and converted into an engineering optimization problem. The ensuing optimization goal is to find a set of parameters in the PV model to minimize the difference between the measured and the computed data. Typically, the root mean square error (RMSE) serves as a metric to quantify the extent of the discrepancy between two data sets. Therefore, the objective function in this context is defined by the RMSE formulation, as in many existing studies [14,56,62,63], as shown in Equation (5).

$$RMSE_i(\boldsymbol{x}) = \sqrt{\frac{1}{N}\sum_{m=1}^{N} f_i(I_m, V_m, \boldsymbol{x})^2} \tag{5}$$

where N expresses the number of measured data, $\boldsymbol{x}$ is a set of unidentified parameters. m indicates the mth measured data of current–voltage. Specifically, f_i (I, V, $\boldsymbol{x}$) represents the error functions of the ith PV model, which is successively defined by Equations (6)–(9).

$$\begin{cases} f_i(I_L, V_L, \boldsymbol{x}) = I_{ph} - I_{sd}\left\{\exp\left[\frac{q(V_L+R_sI_L)}{nkT}\right]-1\right\} - \frac{V_L+R_sI_L}{R_{sh}} - I_L \\ \boldsymbol{x} = [I_{ph}, I_{sd}, R_s, R_{sh}, n] \end{cases} \tag{6}$$

$$\begin{cases} f_i(I_L, V_L, \boldsymbol{x}) = I_{ph} - I_{sd1}\left\{\exp\left[\frac{q(V_L+R_sI_L)}{n_1kT}\right]-1\right\} \\ -I_{sd2}\left\{\exp\left[\frac{q(V_L+R_sI_L)}{n_2kT}\right]-1\right\} \\ -\frac{V_L+R_sI_L}{R_{sh}} - I_L \\ \boldsymbol{x} = [I_{ph}, I_{sd1}, I_{sd2}, R_s, R_{sh}, n_1, n_2] \end{cases} \tag{7}$$

$$\begin{cases} f_i(I_L, V_L, \boldsymbol{x}) = I_{ph} - I_{sd1}\left\{\exp\left[\frac{q(V_L+R_sI_L)}{n_1kT}\right]-1\right\} \\ -I_{sd2}\left\{\exp\left[\frac{q(V_L+R_sI_L)}{n_2kT}\right]-1\right\} - I_{sd3}\left\{\exp\left[\frac{q(V_L+R_sI_L)}{n_3kT}\right]-1\right\} \\ -\frac{V_L+R_sI_L}{R_{sh}} - V_L \\ \boldsymbol{x} = [I_{ph}, I_{sd1}, I_{sd2}, I_{sd3}, R_s, R_{sh}, n_1, n_2, n_3] \end{cases} \tag{8}$$

$$\begin{cases} f_i(I_L, V_L, \boldsymbol{x}) = I_{ph} - I_{sd}\left\{\exp\left[\frac{q(V_L/N_s+R_sI_L/N_p)}{nkT}\right]-1\right\} - \frac{V_L/N_s+R_sI_L/N_p}{R_{sh}} - I_L \\ \boldsymbol{x} = [I_{ph}, I_{sd}, R_s, R_{sh}, n] \end{cases} \tag{9}$$

3. Differential Evolution

Differential evolution (DE) is a simple and effective intelligence optimization algorithm suitable for solving optimization problems in consecutive space. In the population of DE, NP solutions form a population $\boldsymbol{Pop}$, which is indicated by [$\boldsymbol{x}_{1,g}$, $\boldsymbol{x}_{2,g}$, …, $\boldsymbol{x}_{NP,g}$] at the gth generation. Among them, each $\boldsymbol{x}_{i,g}$ (i = 1, 2, …, NP) is encoded as [$x_{i,1,g}$, $x_{i,2,g}$, …, $x_{i,D,g}$], where D represents the decision variable dimension of the unsolved problem. After the random initialization, three operators, i.e., mutation, crossover, and selection, are repeatedly executed to produce the offspring of the whole population for subsequent iterations until satisfying a termination criterion. Specifically, the random initialization is conducted for each individual using Equation (10) at the first iteration.

$$x_{i,j,g} = x_{j,\min} + rand\cdot(x_{j,\max} - x_{j,\min}) \tag{10}$$

where *rand* expresses a random number sampled from the scope [0, 1]; g equals 1 at the first iteration. j indicates an integer from 1 to D; $x_{j,\max}$ and $x_{j,\min}$ respectively represent the top and bottom boundaries of the jth decision variable.

Then, the individual $\boldsymbol{x}_{i,g}$ generates the own mutation vector $\boldsymbol{v}_{i,g}$ by implementing a mutation operator. Three prevalent mutation operators are given as Equations (11)–(13) [64].

(1) DE/rand/1

$$\boldsymbol{v}_{i,g} = \boldsymbol{x}_{r1,g} + F\cdot(\boldsymbol{x}_{r2,g} - \boldsymbol{x}_{r3,g}) \tag{11}$$

(2) DE/best/1

$$\boldsymbol{v}_{i,g} = \boldsymbol{x}_{best,g} + F\cdot(\boldsymbol{x}_{r1,g} - \boldsymbol{x}_{r2,g}) \tag{12}$$

(3) DE/current-to-best/1

$$\boldsymbol{v}_{i,g} = \boldsymbol{x}_{i,g} + F\cdot(\boldsymbol{x}_{best,g} - \boldsymbol{x}_{i,g}) + F\cdot(\boldsymbol{x}_{r1,g} - \boldsymbol{x}_{r2,g}) \tag{13}$$

Among these equations, $\boldsymbol{v}_{i,g}$, produced by a mutation strategy, means the mutator of the individual $\boldsymbol{x}_{i,g}$. $\boldsymbol{x}_{best,g}$ indicates the individual with the best fitness function value at the gth iteration. r_1, r_2, and r_3 are three mutually unequal integers sampled stochastically from 1 to NP. The parameter F is the scaling factor for magnifying differential vectors.

After the mutant operation, each $\boldsymbol{x}_{i,g}$ will generate its trial vector $\boldsymbol{u}_{i,g}$, considered a combination of the mutant vector $\boldsymbol{v}_{i,g}$ and target vector $\boldsymbol{x}_{i,g}$, through conducting the crossover operation. In general, a widely used binomial crossover operation can be described as follows [64]:

$$u_{i,j,g} = \begin{cases} v_{i,j,g}, \text{ if } rand \le CR \text{ or } j = j_{rand} \\ x_{i,j,g}, \text{ otherwise} \end{cases} \tag{14}$$

In Equation (14), *rand* indicates a random number evenly sampled from (0, 1); the parameter CR represents the crossover rate, representing the number of components of the trial vector $\boldsymbol{u}_{i,g}$ from the mutant vector $\boldsymbol{v}_{i,g}$; and j_{rand} is an integer randomly chosen from 1 to D for guaranteeing the existing difference between $\boldsymbol{u}_{i,g}$ and $\boldsymbol{x}_{i,g}$.

Eventually, the selection operation is employed to select an individual with a better fitness value from $\boldsymbol{u}_{i,g}$ and $\boldsymbol{x}_{i,g}$. Considering the minimization nature of the objective function in the PV models, a widely used selection operator is introduced as defined in Equation (15) [64].

$$\boldsymbol{x}_{i,g+1} = \begin{cases} \boldsymbol{u}_{i,g}, \text{ if } f(\boldsymbol{u}_{i,g}) \le f(\boldsymbol{x}_{i,g}) \\ \boldsymbol{x}_{i,g}, \text{ otherwise} \end{cases} \tag{15}$$

where $f\ (\boldsymbol{u}_{i,g})$ and $f\ (\boldsymbol{x}_{i,g})$ respectively represent the fitness values of $\boldsymbol{u}_{i,g}$ and $\boldsymbol{x}_{i,g}$.

4. DODE

This section first elaborates the design motivation of our proposed algorithm. Then, an ensemble of multiple mutation strategies and an orientation guidance mechanism are also expounded in detail. Additionally, other components of the proposed DODE algorithm are listed comprehensively. Finally, the entire procedure of utilizing optimization algorithms to address the parameter identification problem in PV models is presented.

4.1. Motivation

The parameter extraction of PV models is fundamentally a type of multi-modal optimization problem [65], with the primary goal of minimizing the error function value given as Equation (5). This issue usually has numerous local optima, which are immensely challenging for MHAs. To address these multi-modal problems, an algorithm is typically expected to fulfill specific search requirements at different stages [66]. For instance, the exploration capability aids the population in exploring a broader search space, expanding population diversity, and avoiding premature convergence. In contrast, the exploitation capability enables the population to perform refined searches near the optimal solution, enhancing the solving precision. However, for the canonical DE, one single mutation strategy possesses one capability, either exploration or exploitation; thus, it is a challenge to maintain a well-balanced equilibrium between exploration and exploitation. To overcome these deficiencies, a practical and effective approach is incorporating some mutation strategies, compensating for the limitations imposed by a single mutation strategy. This methodology is also commonly referred to as the ensemble method, which has gained significant attention in recent years. Various ensemble DE variants have been developed,

such as multi-role-based DE [67], multi-population ensemble DE [68], and multi-distinct strategy DE [52], to effectively leverage the complementary characteristics of different mutation strategies for solving diverse problem types. These algorithms effectively tackle the problems associated with the ensemble method, particularly concerning strategy pool determination and strategy selection for different individuals or evolutionary stages. However, highly complex algorithms are primarily designed for complicated high-dimensional problems, and the extracted parameters may not always achieve optimal accuracy. For this reason, in this paper an improved differential evolution with a dual mutation strategy collaboration mechanism and an orientation guidance mechanism (DODE) is developed to adaptively allocate mutation strategies to different individuals at different stages and address the multi-modal problem to effectively mitigate the status of populations trapped in local optima. The proposed DODE algorithm incorporates double distinctive strategies similar to the aforementioned ensemble DE variants. However, the difference is that DODE distinguishes itself by employing a straightforward self-adaptive dual mutation strategy collaboration mechanism that achieves a good balance between exploration and exploitation while minimally impacting computational complexity. In addition, an orientation guidance mechanism facilitates the escape of the population's good individuals from local optima during the iterative process, thereby enhancing the solution accuracy.

4.2. Collaboration Mechanism of Dual Mutation Strategies

A collaboration mechanism of dual mutation strategies is developed in the proposed DODE, which integrates two mutation strategies, namely DE/rand/1 and DE/current-to-*p*best/1 [64]. Each mutation strategy serves a specific purpose within the optimization process. Among these, DE/rand/1 is widely regarded as a mutation strategy that enhances the exploration search capability of the population. The second DE/current-to-*p*best/1 is considered a mutation strategy with exploitation inclinations. While selecting mutation strategies serves as a prerequisite for enhancing solution accuracy, the focal point lies in the optimal allocation of both among individuals within the population. From the perspective of the population, it is essential to focus on exploration at the early stages while emphasizing exploitation at the later stages. Moreover, from an individual point of view, each individual plays a specific role due to varying fitness values. Typically, individuals with better fitness values benefit more from a local search to improve the algorithm's solving accuracy. Conversely, other individuals should engage in a global search to maintain population diversity and raise the chances of finding the global optimum solution. For this reason, this paper designs a population-individual-based adaptive mutation strategy collaboration mechanism to balance the search capabilities of the algorithm. Specifically, a parameter γ is defined as shown in Equation (16), which determines the probability of individual $\boldsymbol{x}_{i,g}$ being assigned for global or local searches on the population level.

$$\gamma = \frac{FEs}{MaxFEs} \tag{16}$$

where *FEs* and *MaxFEs* are the current and maximum numbers of fitness evaluations, respectively. As the iteration progresses, the value of γ will increase from 0 to 1. The small value of γ means the algorithm tends to favor exploration; conversely, with a large value, it leans towards exploitation.

In this study, an adaptive factor (*AF*) linked to fitness diversity is developed to characterize the individual status, which can be calculated using the following expression:

$$AF_i = \frac{f(\boldsymbol{x}_{i,g}) - f(\boldsymbol{x}_{best,g}) + \varepsilon}{f(\boldsymbol{x}_{worst,g}) - f(\boldsymbol{x}_{best,g}) + \varepsilon} \tag{17}$$

Herein, $f(\boldsymbol{x}_{i,g})$, $f(\boldsymbol{x}_{worst,g})$, and $f(\boldsymbol{x}_{best,g})$ indicate the fitness function value of the ith individual $\boldsymbol{x}_{i,g}$, the worst individual $\boldsymbol{x}_{worst,g}$, and best individual $\boldsymbol{x}_{best,g}$. ε is defined as a small constant ($\varepsilon = 10^{-20}$) to avoid a denominator of 0.

Combining Equations (16) and (17) allows each $\boldsymbol{x}_{i,g}$ to adaptively select the search mode to generate the mutant vector $\boldsymbol{v}_{i,g}$ at each iteration, as in the following formula:

$$\boldsymbol{v}_{i,g} = \begin{cases} \boldsymbol{x}_{r_1,g} + F_i \times (\boldsymbol{x}_{r_2,g} - \boldsymbol{x}_{r_3,g}), & if\, AF_i > \gamma \\ \boldsymbol{x}_{i,g} + F_i \times (\boldsymbol{x}_{pbest,g} - \boldsymbol{x}_{i,g}) + F_i \times (\boldsymbol{x}_{r_1,g} - \boldsymbol{x}_{r_2,g}), & otherwise \end{cases} \tag{18}$$

where r_1, r_2, and r_3 are three mutually unequal integers sampled uniformly randomly from 1 to NP, and differ from i. $\boldsymbol{x}_{pbest,g}$ represents a stochastically selected member from the top 100 p% of the current population, where the parameter p expresses the proportion of elite individuals in the entire population and is within the range [0, 1].

As illustrated in Figure 5, the number of individuals conducting global searches gradually decreases, while the frequency of local search utilization increases as the iterations progress.

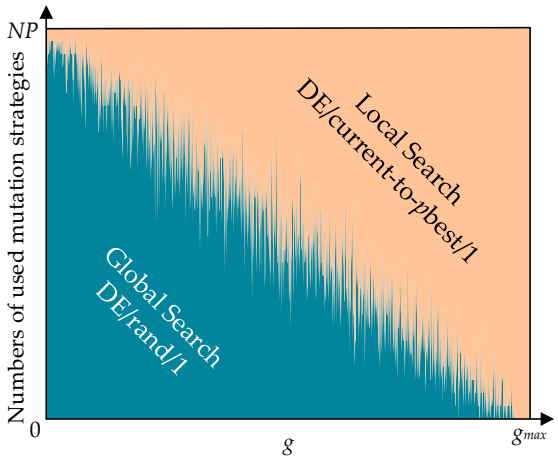

Figure 5. The diagram of the collaboration mechanism of dual mutation strategies.

4.3. Orientation Guidance Mechanism

In solving the parameter identification problem of the PV model, computational resources are often limited. Therefore, individuals with better fitness should be allocated more computational resources during the iteration process to improve the algorithm's solving accuracy. However, for DE algorithms, good individuals are prone to losing their evolution direction and getting trapped in the local optima of the problem. The existing literature often relies on population feedback information for research. For the entire population, its centroid can generally represent the population's position in the solution space. The movement orientation of the centroid can also reflect the evolution trend of the entire population, approximately pointing towards the global optimum of the problem. Thus, this paper proposes a guidance mechanism based on population centroid movement information to aid the further evolution of promising individuals. The diagrammatic sketch of the specific implementation is signified in Figure 6.

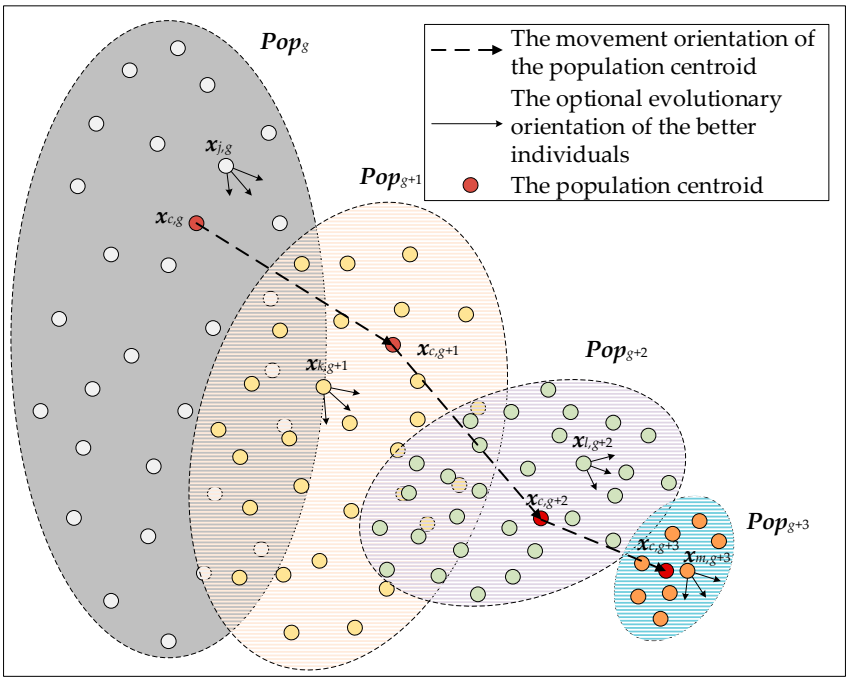

Figure 6. The abridged general view of the proposed orientation guidance mechanism.

In Figure 6, $\boldsymbol{Pop}_g$ indicates the population at the gth generation; $\boldsymbol{x}_{c,g}$ represents the centroid of $\boldsymbol{Pop}_g$, which is calculated by Equation (19). $\boldsymbol{x}_{j,g}$, $\boldsymbol{x}_{k,g+1}$, $\boldsymbol{x}_{l,g+2}$, and $\boldsymbol{x}_{m,g+3}$ respectively represent top four 100 p% individuals with better fitness values in four consecutive generations of evolution. The dashed arrows represent the direction of population centroid evolution. Solid arrows indicate the optional evolution directions of individuals based on the previous centroid evolution direction.

$$\begin{aligned} \boldsymbol{x}_{c,g} &= \sum_{i=1}^{NP} w_i \cdot \boldsymbol{x}_{i,g} \\ w_i &= \frac{AF_i}{\sum_{i=1}^{NP} AF_i} \end{aligned} \tag{19}$$

where ω_i is the weight of the individual fitness value after the normalization processing.

Subsequently, an external archive is employed to store the movement directions of the population centroid (***CM*** for short). When this archive size exceeds NP, the "first-in, first-out" principle removes the earliest stored centroid movement direction. This is because the magnitude of newly generated centroid movement direction vectors gradually decreases as the population iterates. Past differential vectors with larger space spans may not be conducive to the evolution of better individuals in the current population.

Afterward, a group ***PS*** comprises the top 100 p% elite individuals selected from $\boldsymbol{Pop}_g$ for further evolution and utilizes Equation (20) to generate the mutation vector for each elite individual.

$$v_{i,g} = \boldsymbol{PS}_{i,g} + F_i \cdot \boldsymbol{CM}_r \tag{20}$$

where i is an integer from 1 to p*NP, and r is randomly selected from 1 to NP.

Next, these elite individuals undergo crossover and selection operations to generate offspring with better fitness values. Finally, the current population is updated accordingly using Equations (14) and (15). The detailed pseudo-code of the proposed orientation guidance mechanism is presented in Algorithm 1.

Algorithm 1: Orientation guidance mechanism

Input: the current population $\boldsymbol{Pop}$, the current iterations g, the previous centroid $\boldsymbol{x}_{c,g-1}$, the movemernt orientation archive of the centroid $\boldsymbol{CM}$, NP, p, D, $meanF$, $meanCR$

Output: Updated $\boldsymbol{Pop}$, $\boldsymbol{CM}$, $\boldsymbol{x}_{c,g}$

Select the worst and best individuals $\boldsymbol{x}_{worst,g}$ and $\boldsymbol{x}_{best,g}$ from $\boldsymbol{Pop}$
Caculate the current centroid $\boldsymbol{x}_{c,g}$ using Equation (19)
Restore the difference vector $\boldsymbol{x}_{c,g}$ - $\boldsymbol{x}_{c,g-1}$ into $\boldsymbol{CM}$
if $|\boldsymbol{CM}| \geq NP$ **then**
    Remove $|\boldsymbol{CM}|$ - NP individuals stored earlier in $\boldsymbol{CM}$
end
Select the top $100p\%$ individuals from $\boldsymbol{Pop}$ and constitute a group $\boldsymbol{PS}$
Caculate the $F_{i=1\rightarrow p*NP}$ and $\boldsymbol{CR}_{i=1\rightarrow p*NP}$ using Equations (22) and (23)
for i = 1 to p*NP **do**
    Randomly select an integer r from the set of integer [1,2, ..., NP]
    $\boldsymbol{v}_{i,g}$ = $\boldsymbol{PS}_i$ + F_i*$\boldsymbol{CM}_r$
end
Boundary constraint using Equation (21)
Implement the crossover and selection operations for $\boldsymbol{PS}_{i=1\rightarrow NP,g}$ using Equations (14) and (15), respectively
Update $\boldsymbol{Pop}$

4.4. Other Components of DODE

In this subsection, several other aspects of DODE are introduced.

(1) Boundary constraint: The individual from the population may generate mutation vectors that violate the predetermined bound of parameters during the mutation process. Therefore, it is necessary to check and handle the boundary for each mutant vector $v_{i,g}$. The commonly used methods of boundary constraint in EAs include the middle method [69], and the random, projection, and reflection methods [70]. The first method is employed in this paper, expressed as follows:

$$v_{i,j,g} = \begin{cases} (x_{i,j,g} + x_{j,\min})/2, & if\ v_{i,j,g} \leq x_{j,\min} \\ (x_{i,j,g} + x_{j,\max})/2, & else\ v_{i,j,g} \geq x_{j,\max} \\ v_{i,j,g}, & otherwise \end{cases} \tag{21}$$

(2) Associated parameter configurations: In DE, the parameter F amplifies the differential vector, affecting the generated mutant vector. The parameter CR controls the proportion of components sourced from the target vector $\boldsymbol{x}_{i,g}$ and mutant vector $\boldsymbol{v}_{i,g}$ in the trial vector $\boldsymbol{u}_{i,g}$. Both jointly influence the quality of the offspring. Generally, a larger F facilitates exploration, while CR with a larger value accelerates convergence [71]. Therefore, this paper adopts a popular method, proposed in [64], to generate F and CR values. Specifically, the parameters F_i and CR_i for each $\boldsymbol{x}_{i,g}$ are respectively generated by Equations (22) and (23).

$$F_i = randc_i(mean_F, 0.1) \tag{22}$$

$$CR_i = randn_i(mean_{CR}, 0.1) \tag{23}$$

where $randc_i(\mu, \delta^2)$ and $randn_i(\mu, \delta^2)$ are two stochastic numbers that follow a normal distribution and Cauchy distribution with the mean value (μ) and the variance (δ^2). In this paper, $mean_F$ and $mean_{CR}$ are respectively set to be 0.7 and 0.9. The value of F_i and CR_i will be regenerated until meeting the required criteria when they are not within the range of [0, 1].

4.5. DODE Algorithm Procedures

Based on the above theoretical description, the implementation procedures of the proposed DODE are indicated in Algorithm 2. First, the initial population is generated using Equation (10) (Line 1). Then, in the main program loop, the values of γ and $AF_{i=1\to NP}$ are determined through Equations (16) and (17) (Line 7), and all individuals are updated by executing the mutation, crossover, and selection operations according to Equations (14), (15) and (18), respectively (Lines 8–17). Afterward, the orientation guidance mechanism will be implemented and fully utilizes the movement information of the population centroid to further evolve the elite individual, as shown in Algorithm 1. The search task will be continuously performed until fulfilling a presupposed termination criterion.

Algorithm 2: DODE

Input: NP, $MaxFEs$, search dimension D, objective function $f_i(I_L, V_L, \boldsymbol{x})$
Output: The position and fitness of the best solution $\boldsymbol{x}_{best,g}$
`// Initialization`
1 Initialize the individual $\boldsymbol{x}_{i=1\to NP}$ using Equation (10)
2 Evaluate the fitness value of all individuals
3 Obtain the best solution $\boldsymbol{x}_{best,0}$ among $\boldsymbol{Pop}$
4 Caculate the centroid $\boldsymbol{x}_{c,0}$ of $\boldsymbol{Pop}$ using Eq. (19)
5 Set $meanF$ = 0.7, $meanCR$ = 0.9, p = 0.2, c= 0.1, $\boldsymbol{CM} = \varnothing$, $FEs = NP$, g = 1
`// Main Loop`
6 **while** $FEs < MaxFEs$ **do**
7 Caculate the parameters γ and $AF_{i=1\to NP}$ using Equations (16) and (17)
`// Mutation operation`
8 Caculate the $F_{i=1\to NP}$ and $\boldsymbol{CR}_{i=1\to NP}$ using Equations (22) and (23)
9 **for** i = 1 to NP **do**
10 Select the $\boldsymbol{x}_{p,best}$ for the i th individual
11 Randomly select the r_1, r_2 and r_3 from 1 to NP
12 **if** $AF_i \geq \gamma$ **then**
13 $\boldsymbol{v}_{i,g} = \boldsymbol{x}_{r_1,g} + F_i \times (\boldsymbol{x}_{r_2,g} - \boldsymbol{x}_{r_3,g})$
14 **else**
15 $\boldsymbol{v}_{i,g} = \boldsymbol{x}_{i,g} + F_i \times (\boldsymbol{x}_{pbest,g} - \boldsymbol{x}_{i,g}) + F_i \times (\boldsymbol{x}_{r_1,g} - \boldsymbol{x}_{r_2,g})$
16 **end**
17 **end**
18 Boundary constraint using Equation (21)
`// Crossover and Selection operations`
19 Generate $\boldsymbol{u}_{i=1\to NP,g}$ using Equation (14) and evaluate its fitness value
20 Generate $\boldsymbol{x}_{i=1\to NP,g+1}$ by executing the Equation (15)
`// Orientation guidance mechanism`
21 Execute $\boldsymbol{Algorithm}$ 1
22 $FEs = FEs + NP + p*NP$
23 $g = g + 1$
24 **end**

Additionally, the proposed DODE does not visibly increase the total complexity of the classical DE. The accessional complexity of DODE mainly arises from the evolution of elite individuals, as expounded in Algorithm 1 (lines 10–13). The computation complexity of the evolution processes of elite individuals is $O(p \times NP \times D \times G_{max})$, while the complexity of the classical DE is equal to $O(NP \times D \times G_{max})$, where G_{max} indicates the maximum iterations. Therefore, the computation complexity of DODE is $O((1 + p) \times NP \times D \times G_{max}) = O(NP \times D \times G_{max})$, which is the same as in many other DE variants [39,52,53,72]. Actually, our subsequent experimental results also demonstrate that DODE can acquire excellent solutions within a reasonable time of CPU execution.

5. Experiments and Discussions

In this section, six parameter extraction experiments on PV models, encompassing SDM, DDM, TDM, and three PV module models, are conducted to verify the effectiveness of the proposed DODE. The experimental data for SDM, DDM, and TDM, including 26 pairs of current–voltage (*I*-*V*) values [73], are acquired by a 57 mm diameter commercial R.T.C. France silicon solar cell under the irradiance of 1000 W/m^2 at the ambient temperature of 33 °C. The remnant three modules, including Photowatt-PWP201, mono-crystalline STM6-40/36, and poly-crystalline STP6-120/36, assemble 36 poly-crystalline silicon cells in series (i.e., $N_s = 36$, $N_p = 1$) and have been tested at 45 °C, 51 °C, and 55 °C, respectively. The measured values of current–voltage of six PV models stem from [74,75]. The bottom and top limitations for each unidentified variable of six PV models are specified in Table 1 [52,56].

Table 1. The value ranges of parameters of SDM, DDM, TDM, and PV module models.

Parameter	SDM, DDM and TDM	PWP201 Module Model	STM6-40/36 Module Model	STP6-120/36 Module Model
	$[x_{min}, x_{max}]$	$[x_{min}, x_{max}]$	$[x_{min}, x_{max}]$	$[x_{min}, x_{max}]$
I_{ph} (A)	[0, 1]	[0, 2]	[0, 2]	[0, 8]
I_{sd}, I_{sd1}, I_{sd2}, I_{sd3} (μA)	[0, 1]	[0, 50]	[0, 50]	[0, 50]
R_s (Ω)	[0, 100]	[0, 2000]	[0, 1000]	[0, 1500]
R_{sh} (Ω)	[0, 2]	[1, 50]	[1, 60]	[1, 50]
n, n_1, n_2, n_3	[0, 0.5]	[0, 2]	[0, 0.36]	[0, 0.36]

Through a comprehensive comparison with some advanced algorithms, the achieved experiment results were extensively validated in terms of various aspects, encompassing accuracy of parameter identification, errors of extraction results, algorithmic convergence curves, and other relevant indexes. These compared algorithms comprise five DE algorithms (i.e., JADE [64], CoDE [72], MPEDE [68], SEDE [52], and DOLADE [53]) and five other meta-heuristic algorithms (i.e., IWOA [27], PGJAYA [76], IGSK [25], LaPSO [62], and RTLBO [77]). The necessary parameters, configured according to their original papers, and brief introductions of these algorithms, are enumerated in Table 2. For the proposed DODE, the population size NP and parameter p are set to 30 and 0.2, respectively. It is notable that parameter tuning is a difficult task [78]. Thus, a systematical analysis of parameter configurations will be a topic of our future research.

Table 2. Parametric configurations of compared algorithms.

Algorithm	Parameter Setting
JADE	$NP = 100$, $p = 0.05$
CoDE	$NP = 30$
MPEDE	$NP = 100$, $\lambda_1 = \lambda_2 = \lambda_3 = 0.2$, $\Delta = 20$
SEDE	$NP = 30$
DOLADE	$NP = 30$, $\omega = 10$, $p = 0.1$
IWOA	$NP = 50$
PGJAYA	$NP = 20$
IGSK	$NP = 25$
LaPSO	$NP = 40$
RTLBO	$NP = 50$

The proposed DODE and the other ten algorithms were compiled and independently executed 30 times using the MATLAB R2018b platform to ensure an even-handed comparison. The minimum RMSE value among the 30 runs is recorded in the table, along with the corresponding obtained PV model parameters. Additionally, this paper's maximum fitness evaluation number of ten methods is 50,000, as used in many existing studies [29,52,61].

5.1. Simulation Results on Solar Cells

For three solar cells (i.e., SDM, DDM, and TDM), the minimum RMSE values and corresponding extracted parameters of all 11 algorithms are recorded in Tables 3–5 after 30 independent experiments, and the optimal RMSE is marked in bold. In Table 3, five distinct parameters, i.e., I_{ph}, I_{sd}, R_s, R_{sh}, and n, are identified using the different algorithms. It is clear that DODE yields the optimal RMSE value compared to others. In addition, other algorithms (e.g., SEDE, DOLDE, and IGSK) showed good competitiveness but are not up to the level of the proposed DODE. The same observations can be found in Tables 4 and 5, and DODE is still superior to its competitors regarding the RMSE values. It is worth mentioning that although there is little difference in the RMSE among these results, further statistical analysis will reveal the magnitude of the differences between the experimental results of DODE and other algorithms, as shown in Section 5.4.

Table 3. Comparison of the best identified parameters between DODE and its competitors on SDM.

Algorithm	I_{ph} (A)	I_{sd} (μA)	R_s (Ω)	R_{sh} (Ω)	n	RMSE
DODE	0.76077553	0.32302080	0.03637709	53.71852345	1.48118358	**$9.86021877891317 \times 10^{-4}$**
JADE	0.76077553	0.32302083	0.03637709	53.71852601	1.48118359	$9.86021877891517 \times 10^{-4}$
CoDE	0.76077553	0.32302084	0.03637709	53.71853152	1.48118359	$9.86021877891456 \times 10^{-4}$
MPEDE	0.76077553	0.32302080	0.03637709	53.71852047	1.48118358	$9.86021877891538 \times 10^{-4}$
SEDE	0.76077553	0.32302080	0.03637709	53.71852461	1.48118358	$9.86021877891340 \times 10^{-4}$
DOLADE	0.76077553	0.32302082	0.03637709	53.71852583	1.48118359	$9.86021877891336 \times 10^{-4}$
IWOA	0.76077644	0.32272984	0.03638061	53.68727026	1.48109297	$9.86023447010448 \times 10^{-4}$
PGJAYA	0.76077553	0.32301864	0.03637711	53.71834276	1.48118291	$9.86021877975800 \times 10^{-4}$
IGSK	0.76077553	0.32302082	0.03637709	53.71852580	1.48118359	$9.86021877891351 \times 10^{-4}$
LaPSO	0.76077553	0.32302077	0.03637709	53.71852073	1.48118358	$9.86021877891438 \times 10^{-4}$
RTLBO	0.76077559	0.32300375	0.03637731	53.71632309	1.48117830	$9.86021887149475 \times 10^{-4}$

Table 4. Comparison of the best identified parameters between DODE and its competitors on DDM.

Algorithm	I_{ph} (A)	I_{sd1} (μA)	R_s (Ω)	R_{sh} (Ω)	n_1	I_{sd2} (μA)	n_2	RMSE
DODE	0.76078107	0.74934831	0.03674043	55.48544435	2.00000000	0.22597418	1.45101673	**$9.82484851784979 \times 10^{-4}$**
JADE	0.76067398	0.12974901	0.03692816	57.22102685	1.41897076	0.36002573	1.65613462	$1.01024811601081 \times 10^{-3}$
CoDE	0.76078050	0.22611672	0.03674066	55.48967674	1.45106746	0.74784847	1.99999028	$9.82485401810740 \times 10^{-4}$
MPEDE	0.76077534	0.24546787	0.03666342	54.84415319	1.45803750	0.50768799	1.97002060	$9.83127480606161 \times 10^{-4}$
SEDE	0.76078107	0.74934803	0.03674043	55.48544266	2.00000000	0.22597422	1.45101674	$9.82484851785165 \times 10^{-4}$
DOLADE	0.76078107	0.22597405	0.03674043	55.48544128	1.45101668	0.74934913	2.00000000	$9.82484851785086 \times 10^{-4}$
IWOA	0.76077707	0.35203458	0.03653049	54.57562369	1.99999999	0.27558807	1.46771960	$9.83565133991052 \times 10^{-4}$
PGJAYA	0.76077961	0.69818089	0.03670657	55.40297132	2.00000000	0.23236180	1.45336669	$9.82509638915954 \times 10^{-4}$
IGSK	0.76078107	0.22597421	0.03674042	55.48544483	1.45101674	0.74934832	2.00000000	$9.82484851785200 \times 10^{-4}$
LaPSO	0.76078107	0.22597418	0.03674043	55.48544333	1.45101673	0.74934812	2.00000000	$9.82484851785202 \times 10^{-4}$
RTLBO	0.76086000	0.24439194	0.03651828	53.31810159	1.99443815	0.28594618	1.47071319	$9.85473186054530 \times 10^{-4}$

Table 5. Comparison of the best identified parameters between DODE and its competitors on TDM.

Algorithm	I_{ph} (A)	I_{sd1} (μA)	R_s (Ω)	R_{sh} (Ω)	n_1	I_{sd2} (μA)	n_2	I_{sd3} (μA)	n_3	RMSE
DODE	0.76078107	0.22597432	0.03674042	55.48544324	1.45101678	0.25789585	2.00000000	0.49145138	2.00000000	**$9.82484851784993 \times 10^{-4}$**
JADE	0.76062498	0.20071952	0.03729011	59.10391259	1.68060341	0.54865223	1.67338556	0.03422587	1.32770871	$1.00957044428532 \times 10^{-3}$
CoDE	0.76078507	0.10693101	0.03680914	55.80348817	1.82316261	0.68338695	1.97961856	0.20232333	1.44262992	$9.83297746428071 \times 10^{-4}$
MPEDE	0.76076875	0.41048216	0.03679275	55.92712689	1.99828068	0.21128146	1.44557701	0.42974218	1.97766073	$9.82812864303851 \times 10^{-4}$
SEDE	0.76078107	0.73674202	0.03674042	55.48542591	2.00000000	0.01260400	2.00000000	0.22597444	2.00000000	$9.82484851786456 \times 10^{-4}$
DOLADE	0.76078107	0.22597431	0.03674042	55.48543622	1.45101678	0.25182882	2.00000000	0.49751843	2.00000000	$9.82484851785125 \times 10^{-4}$
IWOA	0.76075894	0.27165968	0.03650268	55.13717771	1.46694935	0.37102450	1.99991129	0.01032119	1.69123957	$9.83899673192525 \times 10^{-4}$
PGJAYA	0.76078120	0.67096100	0.03675361	55.54287095	2.00000000	0.22320829	1.44998778	0.10195164	2.00000000	$9.82489030043196 \times 10^{-4}$
IGSK	0.76078107	0.23304941	0.03674043	55.48546231	2.00000000	0.51630172	2.00000000	0.22597394	1.45101665	$9.82484851785564 \times 10^{-4}$
LaPSO	0.76078009	0.83071739	0.03680056	55.75714723	1.99869369	0.13914704	1.43537540	0.08063973	1.47898149	$9.82794807995161 \times 10^{-4}$
RTLBO	0.76075603	0.15689749	0.03636667	53.99399885	1.96768536	0.31744173	1.47987447	0.03722061	1.96416622	$9.86107279748943 \times 10^{-4}$

To further show the solution accuracy of DODE, absolute errors (AEs) of current and power between measured data and identified data are reported in Tables 6 and 7, where AE = $|I_L - I_{ide}|$ or $|P - P_{ide}|$. V_L and I_L represent the measured current–voltage values. P indicates the power according to the measured data. I_{ide} and P_{ide} are the current and power calculated after substituting V_L and the extracted parameters into the corresponding model. The last row of these tables records the sum of AE for this set of identified data.

Table 6. Error metrics of current on each data pair in three solar cell models obtained by DODE.

Item	Measured Data		SDM		DDM		TDM	
			Identified Data		Identified Data		Identified Data	
	V_L (V)	I_L (A)	I_{ide} (A)	AE (A)	I_{ide} (A)	AE (A)	I_{ide} (A)	AE (A)
1	−0.2057	0.7640	0.764088	0.000088	0.763983	0.000017	0.763983	0.000017
2	−0.1291	0.7620	0.762663	0.000663	0.762604	0.000604	0.762604	0.000604
3	−0.0588	0.7605	0.761355	0.000855	0.761337	0.000837	0.761337	0.000837
4	0.0057	0.7605	0.760154	0.000346	0.760174	0.000326	0.760174	0.000326
5	0.0646	0.7600	0.759056	0.000944	0.759108	0.000892	0.759108	0.000892
6	0.1185	0.7590	0.758043	0.000957	0.758122	0.000878	0.758122	0.000878
7	0.1678	0.7570	0.757092	0.000092	0.757188	0.000188	0.757188	0.000188
8	0.2132	0.7570	0.756142	0.000858	0.756244	0.000756	0.756244	0.000756
9	0.2545	0.7555	0.755087	0.000413	0.755178	0.000322	0.755178	0.000322
10	0.2924	0.7540	0.753664	0.000336	0.753723	0.000277	0.753723	0.000277
11	0.3269	0.7505	0.751388	0.000888	0.751396	0.000896	0.751396	0.000896
12	0.3585	0.7465	0.747348	0.000848	0.747296	0.000796	0.747296	0.000796
13	0.3873	0.7385	0.740097	0.001597	0.739991	0.001491	0.739991	0.001491
14	0.4137	0.7280	0.727397	0.000603	0.727265	0.000735	0.727265	0.000735
15	0.4373	0.7065	0.706953	0.000453	0.706836	0.000336	0.706836	0.000336
16	0.4590	0.6755	0.675295	0.000205	0.67523	0.000270	0.675230	0.000270
17	0.4784	0.6320	0.630884	0.001116	0.630888	0.001112	0.630888	0.001112
18	0.4960	0.5730	0.572082	0.000918	0.57214	0.000860	0.572140	0.000860
19	0.5119	0.4990	0.499492	0.000492	0.499571	0.000571	0.499571	0.000571
20	0.5265	0.4130	0.413494	0.000494	0.413556	0.000556	0.413556	0.000556
21	0.5398	0.3165	0.31722	0.000720	0.317242	0.000742	0.317242	0.000742
22	0.5521	0.2120	0.212103	0.000103	0.212081	0.000081	0.212081	0.000081
23	0.5633	0.1035	0.102721	0.000779	0.102672	0.000828	0.102672	0.000828
24	0.5736	−0.0100	−0.00925	0.000751	−0.0093	0.000703	−0.009297	0.000703
25	0.5833	−0.1230	−0.12438	0.001381	−0.12439	0.001390	−0.124390	0.001390
26	0.5900	−0.2100	−0.20919	0.000807	−0.20915	0.000853	−0.209147	0.000853
Total	NA	NA	NA	0.017704	NA	0.017318	NA	0.017319

Table 7. Error metrics of power on each data pair in three solar cell models obtained by DODE.

Item	Measured Data	SDM		DDM		TDM	
		Identified Data		Identified Data		Identified Data	
	P (W)	P_{ide} (W)	AE (W)	P_{ide} (W)	AE (W)	P_{ide} (W)	AE (W)
1	−0.157155	−0.157173	0.000018	−0.157151	0.000003	−0.157151	0.000003
2	−0.098374	−0.098460	0.000086	−0.098452	0.000078	−0.098452	0.000078
3	−0.044717	−0.044768	0.000050	−0.044767	0.000049	−0.044767	0.000049
4	0.004335	0.004333	0.000002	0.004333	0.000002	0.004333	0.000002
5	0.049096	0.049035	0.000061	0.049038	0.000058	0.049038	0.000058
6	0.089942	0.089828	0.000113	0.089837	0.000104	0.089837	0.000104
7	0.127025	0.127040	0.000015	0.127056	0.000032	0.127056	0.000032
8	0.161392	0.161209	0.000183	0.161231	0.000161	0.161231	0.000161
9	0.192275	0.192170	0.000105	0.192193	0.000082	0.192193	0.000082
10	0.220470	0.220371	0.000098	0.220389	0.000081	0.220389	0.000081
11	0.245338	0.245629	0.000290	0.245631	0.000293	0.245631	0.000293
12	0.267620	0.267924	0.000304	0.267906	0.000285	0.267906	0.000285

Table 7. *Cont.*

Item	Measured Data	SDM		DDM		TDM	
		Identified Data		Identified Data		Identified Data	
	P (W)	P_{ide} (W)	AE (W)	P_{ide} (W)	AE (W)	P_{ide} (W)	AE (W)
13	0.286021	0.286640	0.000618	0.286599	0.000578	0.286599	0.000578
14	0.301174	0.300924	0.000250	0.300869	0.000304	0.300869	0.000304
15	0.308952	0.309151	0.000198	0.309099	0.000147	0.309099	0.000147
16	0.310055	0.309960	0.000094	0.309931	0.000124	0.309931	0.000124
17	0.302349	0.301815	0.000534	0.301817	0.000532	0.301817	0.000532
18	0.284208	0.283753	0.000455	0.283782	0.000426	0.283782	0.000426
19	0.255438	0.255690	0.000252	0.255730	0.000292	0.255730	0.000292
20	0.217445	0.217704	0.000260	0.217737	0.000293	0.217737	0.000293
21	0.170847	0.171235	0.000388	0.171247	0.000401	0.171247	0.000401
22	0.117045	0.117102	0.000057	0.117090	0.000045	0.117090	0.000045
23	0.058302	0.057863	0.000439	0.057835	0.000467	0.057835	0.000467
24	−0.005736	−0.005305	0.000431	−0.005333	0.000403	−0.005333	0.000403
25	−0.071746	−0.072552	0.000806	−0.072557	0.000811	−0.072557	0.000811
26	−0.123900	−0.123424	0.000476	−0.123397	0.000503	−0.123397	0.000503
Total	NA	NA	0.006584	NA	0.006554	NA	0.006554

In Table 6, the cumulative AEs of current of the DODE algorithm are 0.017704 A, 0.017318 A, and 0.017319 A for SDM, DDM, and TDM, respectively. Table 7 indicates that the cumulative AEs of power of three solar cells obtained by DODE are 0.006584 W, 0.006554 W, and 0.006554 W, respectively. All these experimental data demonstrate that DODE achieves higher accuracy in parameter extraction for SDM, DDM, and TDM.

As a further analysis, Figure 7a–c depict the fitting results using the parameters identified by DODE for each model. These curves represent the fitted *I*-*V* and *P*-*V* characteristics, while the solid dots represent the measured data. The current and power results identified through DODE are highly consistent with the measured results at different voltage levels, which explicitly demonstrates that the unidentified parameter values obtained by DODE are also highly accurate.

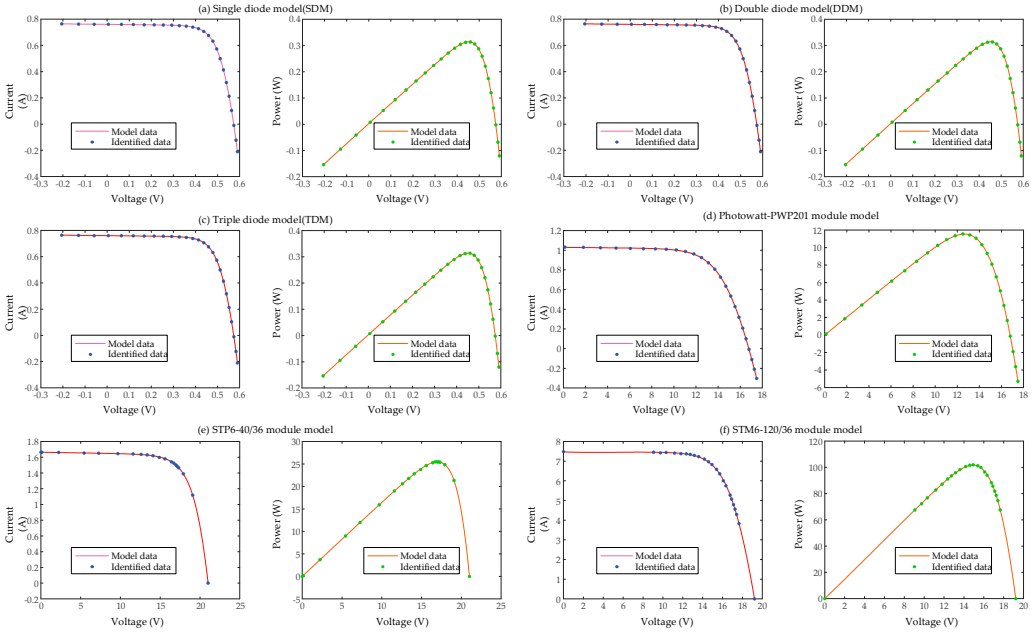

Figure 7. The comparison between the identified data and measured data on (**a**) SDM, (**b**) DDM, (**c**) TDM, (**d**) Photowatt-PWP201 module model, (**e**) STM6-40/36 module model, and (**f**) STP6-120/36 module model by DODE.

5.2. Simulation Results on PV Models

Based on the previous description, five common parameters must be accurately identified for three PV module models (i.e., Photowatt-PWP201, STM6-40/36, and STP6-120/36). The minimum RMSE and the associated parameter identification results are recorded in Tables 8–10. For the first module, DODE yields the optimal RMSE value of $2.42507486809489 \times 10^{-3}$, while IGSK and DOLADE rank second and third with RMSE values of $2.42507486809494 \times 10^{-3}$ and $2.42507486809496 \times 10^{-3}$, respectively. DODE still performs the best among all 11 algorithms for the last two module models. Furthermore, SEDE, DOLADE, and IGSK obtain RMSE values closest to the best result of DODE, while MPEDE, IWOA, RTLBO, and JADE perform poorly. Subsequent statistical tests also support this observation.

Table 8. Comparison of the best identified parameters between DODE and its competitors on the Photowatt-PWP201 module model.

Algorithm	I_{ph} (A)	I_{sd} (μA)	R_s (Ω)	R_{sh} (Ω)	n	RMSE
DODE	1.03051429	3.48226281	0.03336863	27.27728478	1.35118985	**$2.42507486809489 \times 10^{-3}$**
JADE	1.03051428	3.48226639	0.03336863	27.27733451	1.35118996	$2.42507486810290 \times 10^{-3}$
CoDE	1.03051429	3.48226251	0.03336863	27.27728076	1.35118984	$2.42507486809513 \times 10^{-3}$
MPEDE	1.03054243	3.48956784	0.03336176	27.23598089	1.35141512	$2.42511061997362 \times 10^{-3}$
SEDE	1.03051429	3.48226268	0.03336863	27.27728146	1.35118985	$2.42507486809497 \times 10^{-3}$
DOLADE	1.03051429	3.48226306	0.03336863	27.27728618	1.35118986	$2.42507486809496 \times 10^{-3}$
IWOA	1.03040809	3.54744628	0.03331584	27.85625694	1.35316311	$2.42561743308710 \times 10^{-3}$
PGJAYA	1.03050579	3.48485479	0.03336674	27.31298856	1.35126845	$2.42507609902024 \times 10^{-3}$
IGSK	1.03051429	3.48226294	0.03336863	27.27728509	1.35118985	$2.42507486809494 \times 10^{-3}$
LaPSO	1.03051429	3.48226265	0.03336863	27.27728259	1.35118984	$2.42507486809501 \times 10^{-3}$
RTLBO	1.03015603	3.65467583	0.03323196	29.06522817	1.35633820	$2.42889439046789 \times 10^{-3}$

Table 9. Comparison of the best identified parameters between DODE and its competitors on the STM6-40/36 module model.

Algorithm	I_{ph} (A)	I_{sd} (μA)	R_s (Ω)	R_{sh} (Ω)	n	RMSE
DODE	1.66390477	1.73865688	0.00427377	15.92829407	1.52030292	**$1.72981370994064 \times 10^{-3}$**
JADE	1.66390477	1.73865757	0.00427376	15.92829274	1.52030296	$1.72981370994262 \times 10^{-3}$
CoDE	1.66390477	1.73865694	0.00427377	15.92829435	1.52030292	$1.72981370994069 \times 10^{-3}$
MPEDE	1.66390498	1.73863131	0.00427383	15.92814251	1.52030131	$1.72981371268042 \times 10^{-3}$
SEDE	1.66390477	1.73865685	0.00427377	15.92829397	1.52030291	$1.72981370994066 \times 10^{-3}$
DOLADE	1.66390477	1.73865684	0.00427377	15.92829398	1.52030291	$1.72981370994066 \times 10^{-3}$
IWOA	1.66379614	1.81066869	0.00414465	16.14014430	1.52477703	$1.73243299926313 \times 10^{-3}$
PGJAYA	1.66390384	1.73934908	0.00427256	15.93036937	1.52034667	$1.72981397145254 \times 10^{-3}$
IGSK	1.66390477	1.73865694	0.00427377	15.92829441	1.52030292	$1.72981370994066 \times 10^{-3}$
LaPSO	1.66390477	1.73865692	0.00427377	15.92829419	1.52030292	$1.72981370994068 \times 10^{-3}$
RTLBO	1.66391291	1.73747384	0.00427599	15.92088666	1.52022818	$1.72981674269726 \times 10^{-3}$

Table 10. Comparison of the best identified parameters between DODE and its competitors on the STP6-120/36 module model.

Algorithm	I_{ph} (A)	I_{sd} (μA)	R_s (Ω)	R_{sh} (Ω)	n	RMSE
DODE	7.47252991	2.33499508	0.00459463	22.21990866	1.26010347	**$1.66006031250846 \times 10^{-2}$**
JADE	7.47253043	2.33503709	0.00459462	22.22041348	1.26010497	$1.66006031304504 \times 10^{-2}$
CoDE	7.47252992	2.33499488	0.00459463	22.21988727	1.26010347	$1.66006031250856 \times 10^{-2}$
MPEDE	7.47214066	2.37215167	0.00458792	23.35835020	1.26142916	$1.66022624048459 \times 10^{-2}$
SEDE	7.47252992	2.33499498	0.00459463	22.21989817	1.26010347	$1.66006031250850 \times 10^{-2}$
DOLADE	7.47252991	2.33499510	0.00459463	22.21990561	1.26010347	$1.66006031250848 \times 10^{-2}$
IWOA	7.47238198	2.34554850	0.00459257	22.58549502	1.26047966	$1.66007104108898 \times 10^{-2}$

Table 10. *Cont.*

Algorithm	I_{ph} (A)	I_{sd} (μA)	R_s (Ω)	R_{sh} (Ω)	n	RMSE
PGJAYA	7.47253547	2.33529083	0.00459457	22.21637131	1.26011413	$1.66006033230863 \times 10^{-2}$
IGSK	7.47252992	2.33499484	0.00459463	22.21989954	1.26010347	$1.66006031250849 \times 10^{-2}$
LaPSO	7.47252991	2.33499511	0.00459463	22.21991049	1.26010348	$1.66006031250853 \times 10^{-2}$
RTLBO	7.47245448	2.33757248	0.00459403	22.34022389	1.26019578	$1.66006281589215 \times 10^{-2}$

Tables 11 and 12 report the AEs of current and power between the identified and measured values for these three PV modules. Intuitively, the cumulative AE increases accordingly as the model becomes more complex. The maximum AE of current and power is 0.277976 A and 3.911436 W, respectively, obtained from the simulation results of the third model.

Table 11. Error metrics of current on each data pair in three PV module models obtained by DODE.

Item	PWP201 Module Model				STM6-30/36 Module Model				STP6-120/36 Module Model			
	Measured Data		Identified Data		Measured Data		Identified Data		Measured Data		Identified Data	
	V_L (V)	I_L (A)	I_{ide} (A)	AE (A)	V_L (V)	I_L (A)	I_{ide} (A)	AE (A)	V_L (V)	I_L (A)	I_{ide} (A)	AE (A)
1	0.1248	1.0315	1.029122	0.002378	0.000	1.663	1.663458	0.000458	19.21	0.00	0.001164	0.001164
2	1.8093	1.03	1.027384	0.002616	0.118	1.663	1.663252	0.000252	17.65	3.83	3.832282	0.002282
3	3.3511	1.026	1.025742	0.000258	2.237	1.661	1.659551	0.001449	17.41	4.29	4.273929	0.016071
4	4.7622	1.022	1.024104	0.002104	5.434	1.653	1.653914	0.000914	17.25	4.56	4.546289	0.013711
5	6.0538	1.018	1.022283	0.004283	7.260	1.650	1.650566	0.000566	17.10	4.79	4.785833	0.004167
6	7.2364	1.0155	1.019917	0.004417	9.680	1.645	1.645430	0.000430	16.90	5.07	5.081934	0.011934
7	8.3189	1.014	1.016351	0.002351	11.590	1.640	1.639234	0.000766	16.76	5.27	5.273765	0.003765
8	9.3097	1.01	1.010491	0.000491	12.600	1.636	1.633715	0.002285	16.34	5.75	5.776814	0.026814
9	10.2163	1.0035	1.000679	0.002821	13.370	1.629	1.627288	0.001712	16.08	6.00	6.037492	0.037492
10	11.0449	0.988	0.984653	0.003347	14.090	1.619	1.618315	0.000685	15.71	6.36	6.348727	0.011273
11	11.8018	0.963	0.959697	0.003303	14.880	1.597	1.603067	0.006067	15.39	6.58	6.567929	0.012071
12	12.4929	0.9255	0.923049	0.002451	15.590	1.581	1.581585	0.000585	14.93	6.83	6.814860	0.015140
13	13.1231	0.8725	0.872588	0.000088	16.400	1.542	1.542327	0.000327	14.58	6.97	6.958449	0.011551
14	13.6983	0.8075	0.807310	0.000190	16.710	1.524	1.521225	0.002775	14.17	7.10	7.088137	0.011863
15	14.2221	0.7265	0.727958	0.001458	16.980	1.500	1.499206	0.000794	13.59	7.23	7.217761	0.012239
16	14.6995	0.6345	0.636466	0.001966	17.130	1.485	1.485271	0.000271	13.16	7.29	7.284130	0.005870
17	15.1346	0.5345	0.535696	0.001196	17.320	1.465	1.465643	0.000643	12.74	7.34	7.331483	0.008517
18	15.5311	0.4275	0.428816	0.001316	17.910	1.388	1.387599	0.000401	12.36	7.37	7.363265	0.006735
19	15.8929	0.3185	0.318669	0.000169	19.080	1.118	1.118372	0.000372	11.81	7.38	7.395873	0.015873
20	16.2229	0.2085	0.207857	0.000643	21.020	0.000	−0.000021	0.000021	11.17	7.41	7.420265	0.010265
21	16.5241	0.101	0.098354	0.002646	NA	NA	NA	NA	10.32	7.44	7.439092	0.000908
22	16.7987	−0.008	−0.008169	0.000169	NA	NA	NA	NA	9.74	7.42	7.446715	0.026715
23	17.0499	−0.111	−0.110968	0.000032	NA	NA	NA	NA	9.06	7.45	7.452538	0.002538
24	17.2793	−0.209	−0.209118	0.000118	NA	NA	NA	NA	0.00	7.48	7.470981	0.009019
25	17.4885	−0.303	−0.302022	0.000978	NA	NA	NA	NA	NA	NA	NA	NA
Total	NA	NA	NA	0.041788	NA	NA	NA	0.021775	NA	NA	NA	0.277976

Table 12. Error metrics of power on each data pair in three PV module models obtained by DODE.

Item	PWP201 Module Model			STM6-30/36 Module Model			STP6-120/36 Module Model		
	Measured Data	Identified Data		Measured Data	Identified Data		Measured Data	Identified Data	
	P (W)	P_{ide} (W)	AE (W)	P (W)	P_{ide} (W)	AE (W)	P (W)	P_{ide} (W)	AE (W)
1	0.128731	0.128434	0.000297	0.000000	0.000000	0.000000	0.000000	0.022367	0.022367
2	1.863579	1.858847	0.004732	0.196234	0.196264	0.000030	67.599500	67.639783	0.040283

Table 12. *Cont.*

Item	PWP201 Module Model			STM6-30/36 Module Model			STP6-120/36 Module Model		
	Measured Data	Identified Data		Measured Data	Identified Data		Measured Data	Identified Data	
	P (W)	P_{ide} (W)	AE (W)	P (W)	P_{ide} (W)	AE (W)	P (W)	P_{ide} (W)	AE (W)
3	3.438229	3.437364	0.000864	3.715657	3.712416	0.003241	74.688900	74.409105	0.279795
4	4.866968	4.876988	0.010020	8.982402	8.987371	0.004969	78.660000	78.423492	0.236508
5	6.162768	6.188699	0.025931	11.979000	11.983107	0.004107	81.909000	81.837745	0.071255
6	7.348564	7.380530	0.031966	15.923600	15.927767	0.004167	85.683000	85.884683	0.201683
7	8.435365	8.454921	0.019556	19.007600	18.998723	0.008877	88.325200	88.388304	0.063104
8	9.402797	9.407372	0.004575	20.613600	20.584810	0.028790	93.955000	94.393138	0.438138
9	10.252057	10.223234	0.028823	21.779730	21.756847	0.022883	96.480000	97.082878	0.602878
10	10.912361	10.875398	0.036963	22.811710	22.802061	0.009649	99.915600	99.738508	0.177092
11	11.365133	11.326157	0.038977	23.763360	23.853643	0.090283	101.266200	101.080433	0.185767
12	11.562179	11.531556	0.030623	24.647790	24.656910	0.009120	101.971900	101.745861	0.226039
13	11.449905	11.451062	0.001157	25.288800	25.294170	0.005370	101.622600	101.454187	0.168413
14	11.061377	11.058776	0.002601	25.466040	25.419669	0.046371	100.607000	100.438906	0.168094
15	10.332356	10.353089	0.020733	25.470000	25.456513	0.013487	98.255700	98.089367	0.166333
16	9.326833	9.355735	0.028902	25.438050	25.442695	0.004645	95.936400	95.859149	0.077251
17	8.089444	8.107546	0.018102	25.373800	25.384940	0.011140	93.511600	93.403094	0.108506
18	6.639545	6.659986	0.020441	24.859080	24.851904	0.007176	91.093200	91.009953	0.083247
19	5.061889	5.064569	0.002680	21.331440	21.338540	0.007100	87.157800	87.345262	0.187462
20	3.382475	3.372045	0.010429	0.000000	−0.000448	0.000448	82.769700	82.884360	0.114660
21	1.668934	1.625215	0.043719	NA	NA	NA	76.780800	76.771432	0.009368
22	−0.134390	−0.137234	0.002845	NA	NA	NA	72.270800	72.531004	0.260204
23	−1.892539	−1.892001	0.000538	NA	NA	NA	67.497000	67.519990	0.022990
24	−3.611374	−3.613406	0.002032	NA	NA	NA	0.000000	0.000000	0.000000
25	−5.299016	−5.281918	0.017097	NA	NA	NA	NA	NA	NA
Total	NA	NA	0.404604	NA	NA	0.281852	NA	NA	3.911436

Additionally, Figure 7d–f respectively depict the curves of *I*-*V* and *P*-*V* according to the extracted parameters through DODE for the Photowatt-PWP201, STM6-40/36, and STP6-120/36 module models, illustrating that, even with complex models, DODE can closely approximate the actual experimental data. Therefore, this provides a reference and research foundation for accurately obtaining PV model parameters and ensuring the construction of PV models and the secure and steady work of PV systems.

5.3. Convergence Characteristic Analysis

According to the above discussion, it can be found that the proposed DODE performs better on the six PV models above than other methods. To gain a deeper insight into the dynamic search process of all tested algorithms, the convergence characteristic graphs of all tested algorithms are illustrated in Figure 8, with a varying number of fitness evaluations, from which the proposed DODE converges faster than all competitors in six cases. It is noteworthy that the convergence characteristic of DODE shows a slow convergence rate in the early iterations and, after that, it quickly converges to the global optimum. The main reason for this phenomenon is that DODE fully exerts the superiorities of the collaboration and orientation guidance mechanisms, increasing the chances of discovering the global optimum via the guidance of elites when realizing an equilibrium between exploration and exploitation, thus enhancing its search performance.

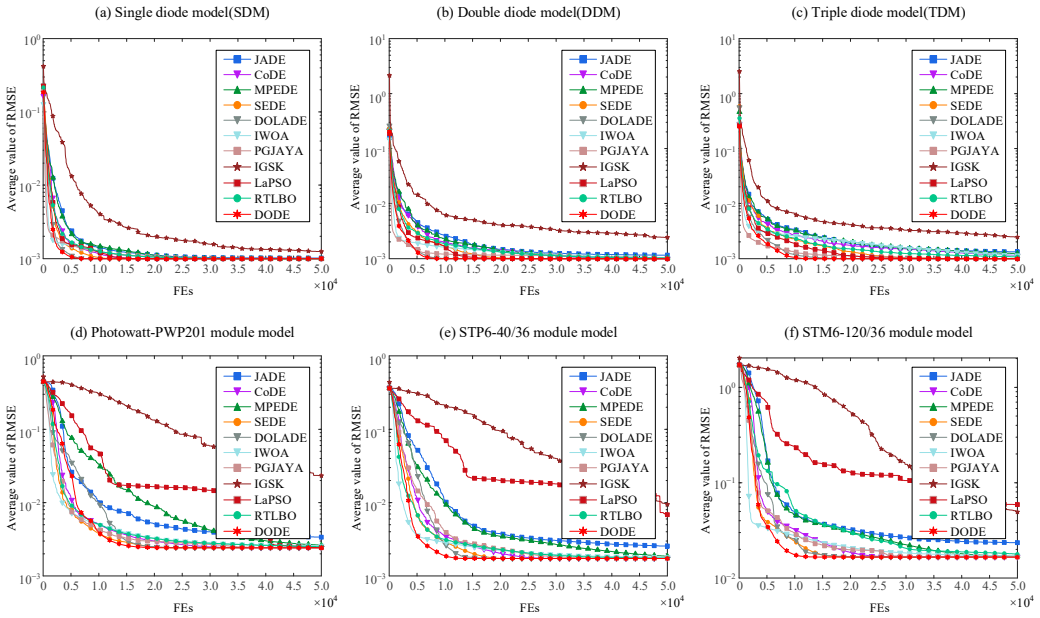

Figure 8. Convergence characteristic curves of all 11 tested algorithms.

5.4. Statistical Results

In this subsection, the statistical results based on the above experiment data are also elaborated to further verify the performance of DODE. The worst, best, and average values and the standard deviation of the RMSE among thirty independent tests are respectively represented by Max, Min, Mean, and SD for SDM, DDM, TDM, Photowatt-PWP201, STP6-120/36, and STM6-40/36 module models, as reported in Table 13, and minimum values are marked in bold. Furthermore, the Wilcoxon rank-sum test [79], a non-parametric test method, is conducted to judge whether there is statistical significance between DODE and its opponents under a significance level $\alpha = 0.05$. To facilitate observation, the signs, i.e., "+", "−", and "=", respectively signify that the performance of DODE is significantly better than, inferior to, and not significantly different from the compared algorithm. The p-value is used for assessing the difference between the proposed DODE and its competitor. If the p-value is greater than or equal to α, there is a non-significant difference between DODE and ten competitors, and vice versa. Observations can be made from Table 13, as follows:

(1) For SDM, DODE yields the minimum Min and Mean values, indicating that it performs the best among 30 independent runs. DOLADE obtains the best Max and SD values, suggesting that it possesses the best robustness compared to others. Moreover, Wilcoxon rank-sum test results indicate that DODE is significantly superior to other competitors.

(2) For DDM, DODE computes the best Max and Min values, while SEDE obtains the best Mean and SD. Wilcoxon rank-sum test results indicate that DODE significantly outdoes other algorithms.

(3) For TDM, we can observe that DODE attains the minimum on all four indexes. Moreover, all p-values indicate that DODE is significantly superior to others.

(4) For the Photowatt-PWP201 module model, DODE obtains the optimal values on Max, Min, and Mean, while SEDE possesses the same Mean as DODE and finds the best SD. In addition, the statistical results indicate that DODE is tied with SEDE, DOLADE, and IGSK, while is better than the remaining models.

(5) For the STM6-40/36 module model, DODE still possesses the best Max, Min, and Mean on four indexes, but SEDE, DOLADE, and IGSK achieve the Max and Mean values, which is the same as DODE. DOLADE has the best SD value. All p-values indicate that DODE significantly outperforms the others.

Table 13. Statistical results on six types of PV models obtained by all 11 tested algorithms.

Model	Algorithm	Max	Min	Mean	SD	Rank-Sum	*p*-Value
SDM	DODE	$9.86021877891504 \times 10^{-4}$	$\mathbf{9.86021877891317 \times 10^{-4}}$	$\mathbf{9.86021877891411 \times 10^{-4}}$	$4.76436810281140 \times 10^{-17}$	NA	NA
	JADE	$1.15321521879939 \times 10^{-3}$	$9.86021877891517 \times 10^{-4}$	$1.00716648820523 \times 10^{-3}$	$3.77565829307664 \times 10^{-5}$	(+)	1.4295×10^{-11}
	CoDE	$9.86021877891586 \times 10^{-4}$	$9.86021877891456 \times 10^{-4}$	$9.86021877891509 \times 10^{-4}$	$4.79538261673457 \times 10^{-17}$	(+)	7.4114×10^{-10}
	MPEDE	$9.86021909426073 \times 10^{-4}$	$9.86021877891538 \times 10^{-4}$	$9.86021879042075 \times 10^{-4}$	$5.64988986709267 \times 10^{-12}$	(+)	1.3764×10^{-11}
	SEDE	$9.86021877891605 \times 10^{-4}$	$9.86021877891340 \times 10^{-4}$	$9.86021877891462 \times 10^{-4}$	$7.47323394301810 \times 10^{-17}$	(+)	8.3835×10^{-3}
	DOLADE	$\mathbf{9.86021877891487 \times 10^{-4}}$	$9.86021877891336 \times 10^{-4}$	$9.86021877891437 \times 10^{-4}$	$\mathbf{3.86051697701479 \times 10^{-17}}$	(+)	1.3967×10^{-2}
	IWOA	$9.87725092480884 \times 10^{-4}$	$9.86023447010448 \times 10^{-4}$	$9.86542108579345 \times 10^{-4}$	$5.30057786071925 \times 10^{-7}$	(+)	1.4295×10^{-11}
	PGJAYA	$9.87580920047622 \times 10^{-4}$	$9.86021877975800 \times 10^{-4}$	$9.86076703117466 \times 10^{-4}$	$2.79467318577159 \times 10^{-7}$	(+)	1.4215×10^{-11}
	IGSK	$9.86021877891559 \times 10^{-4}$	$9.86021877891351 \times 10^{-4}$	$9.86021877891483 \times 10^{-4}$	$4.56882160846755 \times 10^{-17}$	(+)	3.6312×10^{-7}
	LaPSO	$9.86021877893221 \times 10^{-4}$	$9.86021877891438 \times 10^{-4}$	$9.86021877891614 \times 10^{-4}$	$4.30215181759160 \times 10^{-16}$	(+)	4.6566×10^{-09}
	RTLBO	$9.95102691642195 \times 10^{-4}$	$9.86021887149475 \times 10^{-4}$	$9.87840663850941 \times 10^{-4}$	$2.66267998863458 \times 10^{-6}$	(+)	1.4295×10^{-11}
DDM	DODE	$\mathbf{9.86021877891492 \times 10^{-4}}$	$\mathbf{9.82484851784979 \times 10^{-4}}$	$9.83192257013672 \times 10^{-4}$	$1.41481043888143 \times 10^{-6}$	NA	NA
	JADE	$1.46814244601502 \times 10^{-3}$	$1.01024811601081 \times 10^{-3}$	$1.13980772164520 \times 10^{-3}$	$1.19243382122062 \times 10^{-4}$	(+)	1.5080×10^{-11}
	CoDE	$1.01499195548530 \times 10^{-3}$	$9.82485401810740 \times 10^{-4}$	$9.85111165917372 \times 10^{-4}$	$5.77241006989757 \times 10^{-6}$	(+)	7.0983×10^{-6}
	MPEDE	$1.34000615699996 \times 10^{-3}$	$9.83127480606161 \times 10^{-4}$	$1.02442669329253 \times 10^{-3}$	$9.08861171340222 \times 10^{-5}$	(+)	1.9593×10^{-08}
	SEDE	$9.86021877891738 \times 10^{-4}$	$9.82484851785165 \times 10^{-4}$	$\mathbf{9.82818237549593 \times 10^{-4}}$	$\mathbf{8.76073669368551 \times 10^{-7}}$	(+)	7.9047×10^{-5}
	DOLADE	$9.86021877891541 \times 10^{-4}$	$9.82484851785086 \times 10^{-4}$	$9.83310157876682 \times 10^{-4}$	$1.49599433374805 \times 10^{-6}$	(+)	8.4759×10^{-3}
	IWOA	$1.13335738158299 \times 10^{-3}$	$9.83565133991052 \times 10^{-4}$	$1.02006932208289 \times 10^{-3}$	$3.83500358428075 \times 10^{-5}$	(+)	4.9563×10^{-11}
	PGJAYA	$1.00293802399594 \times 10^{-3}$	$9.82509638915954 \times 10^{-4}$	$9.87716183405791 \times 10^{-4}$	$6.01377634281004 \times 10^{-6}$	(+)	5.2220×10^{-7}
	IGSK	$9.86021877891651 \times 10^{-4}$	$9.82484851785200 \times 10^{-4}$	$9.83604169353349 \times 10^{-4}$	$1.56896272503491 \times 10^{-6}$	(+)	3.5835×10^{-5}
	LaPSO	$9.86021877891546 \times 10^{-4}$	$9.82484851785202 \times 10^{-4}$	$9.82947554729584 \times 10^{-4}$	$1.12627926284723 \times 10^{-6}$	(+)	2.1580×10^{-4}
	RTLBO	$1.22611480866827 \times 10^{-3}$	$9.85473186054530 \times 10^{-4}$	$1.01370580449482 \times 10^{-3}$	$5.43795142813846 \times 10^{-5}$	(+)	2.7848×10^{-10}
TDM	DODE	$\mathbf{9.86012141842487 \times 10^{-4}}$	$\mathbf{9.82484851784993 \times 10^{-4}}$	$\mathbf{9.82779670496747 \times 10^{-4}}$	$\mathbf{9.09172775217468 \times 10^{-7}}$	NA	NA
	JADE	$2.16528593256465 \times 10^{-3}$	$1.00957044428532 \times 10^{-3}$	$1.31035319578759 \times 10^{-3}$	$2.80955042829955 \times 10^{-4}$	(+)	1.4323×10^{-11}
	CoDE	$1.60121397248637 \times 10^{-3}$	$9.83297746428071 \times 10^{-4}$	$1.13233460449822 \times 10^{-3}$	$1.65683169893251 \times 10^{-4}$	(+)	5.1287×10^{-11}
	MPEDE	$1.91307457676052 \times 10^{-3}$	$9.82812864303851 \times 10^{-4}$	$1.22768988322227 \times 10^{-3}$	$2.56066083663204 \times 10^{-4}$	(+)	1.1000×10^{-10}
	SEDE	$9.87089713674037 \times 10^{-4}$	$9.82484851786456 \times 10^{-4}$	$9.83811328146404 \times 10^{-4}$	$1.35211644958480 \times 10^{-6}$	(+)	6.0062×10^{-08}
	DOLADE	$9.86022468500695 \times 10^{-4}$	$9.82484851785125 \times 10^{-4}$	$9.82880739811767 \times 10^{-4}$	$9.74800440804199 \times 10^{-7}$	(+)	6.7632×10^{-4}
	IWOA	$1.40409074266789 \times 10^{-3}$	$9.83899673192525 \times 10^{-4}$	$1.13647517747175 \times 10^{-3}$	$1.00393239077011 \times 10^{-4}$	(+)	1.7933×10^{-11}
	PGJAYA	$1.02121272228188 \times 10^{-3}$	$9.82489030043196 \times 10^{-4}$	$9.89231006684404 \times 10^{-4}$	$7.25801161236792 \times 10^{-6}$	(+)	5.4929×10^{-10}
	IGSK	$9.86260741972316 \times 10^{-4}$	$9.82484851785564 \times 10^{-4}$	$9.83175863594395 \times 10^{-4}$	$1.03902873723312 \times 10^{-6}$	(+)	2.3125×10^{-7}
	LaPSO	$9.93795049283600 \times 10^{-4}$	$9.82794807995161 \times 10^{-4}$	$9.85009173705836 \times 10^{-4}$	$2.74816286005806 \times 10^{-6}$	(+)	3.3486×10^{-09}
	RTLBO	$1.37091043098428 \times 10^{-3}$	$9.86107279748943 \times 10^{-4}$	$1.06361165053575 \times 10^{-3}$	$9.15672794543958 \times 10^{-5}$	(+)	1.4323×10^{-11}

Table 13. *Cont.*

Model	Algorithm	Max	Min	Mean	SD	Rank-Sum	*p*-Value
PWP201	DODE	$\mathbf{2.42507486809506 \times 10^{-3}}$	$\mathbf{2.42507486809489 \times 10^{-3}}$	$\mathbf{2.42507486809502 \times 10^{-3}}$	$4.10461626212945 \times 10^{-17}$	NA	NA
	JADE	$4.98633818165731 \times 10^{-3}$	$2.42507486810290 \times 10^{-3}$	$3.37970959170571 \times 10^{-3}$	$8.99516975676339 \times 10^{-4}$	(+)	1.4780×10^{-11}
	CoDE	$2.42507486870952 \times 10^{-3}$	$2.42507486809513 \times 10^{-3}$	$2.42507486811983 \times 10^{-3}$	$1.09710461288146 \times 10^{-13}$	(+)	1.4486×10^{-11}
	MPEDE	$3.10284947721046 \times 10^{-3}$	$2.42511061997362 \times 10^{-3}$	$2.62786165767249 \times 10^{-3}$	$2.16785092840004 \times 10^{-4}$	(+)	1.4215×10^{-11}
	SEDE	$2.42507486809511 \times 10^{-3}$	$2.42507486809497 \times 10^{-3}$	$\mathbf{2.42507486809502 \times 10^{-3}}$	$\mathbf{3.35024202198999 \times 10^{-17}}$	(≈)	1.8029×10^{-1}
	DOLADE	$2.42507486809510 \times 10^{-3}$	$2.42507486809496 \times 10^{-3}$	$2.42507486809503 \times 10^{-3}$	$3.40672816423479 \times 10^{-17}$	(≈)	4.8226×10^{-1}
	IWOA	$2.91760303354987 \times 10^{-3}$	$2.42561743308710 \times 10^{-3}$	$2.58985585802751 \times 10^{-3}$	$1.07274004071403 \times 10^{-4}$	(+)	1.4780×10^{-11}
	PGJAYA	$2.44840305719686 \times 10^{-3}$	$2.42507609902024 \times 10^{-3}$	$2.43149698978649 \times 10^{-3}$	$8.73626139992579 \times 10^{-6}$	(+)	1.4550×10^{-11}
	IGSK	$2.42507486809511 \times 10^{-3}$	$2.42507486809494 \times 10^{-3}$	$2.42507486809503 \times 10^{-3}$	$3.87004392342166 \times 10^{-17}$	(≈)	7.4480×10^{-1}
	LaPSO	$3.04703699752841 \times 10^{-3}$	$2.42507486809501 \times 10^{-3}$	$2.44580693907619 \times 10^{-3}$	$1.11645619026492 \times 10^{-4}$	(+)	4.7641×10^{-08}
	RTLBO	$2.70490127586173 \times 10^{-3}$	$2.42889439046789 \times 10^{-3}$	$2.50904999738576 \times 10^{-3}$	$7.63295710664747 \times 10^{-5}$	(+)	1.4780×10^{-11}
STM6-40/36	DODE	$\mathbf{1.72981370994070 \times 10^{-3}}$	$\mathbf{1.72981370994064 \times 10^{-3}}$	$\mathbf{1.72981370994068 \times 10^{-3}}$	$1.27675873707146 \times 10^{-17}$	NA	NA
	JADE	$3.27263799793268 \times 10^{-3}$	$1.72981370994262 \times 10^{-3}$	$2.55458258766248 \times 10^{-3}$	$4.68082127878847 \times 10^{-4}$	(+)	1.4295×10^{-11}
	CoDE	$1.72981370994073 \times 10^{-3}$	$1.72981370994069 \times 10^{-3}$	$1.72981370994071 \times 10^{-3}$	$9.79125207905825 \times 10^{-18}$	(+)	5.5889×10^{-11}
	MPEDE	$2.19736357651583 \times 10^{-3}$	$1.72981371268042 \times 10^{-3}$	$1.85867139058643 \times 10^{-3}$	$1.17777494798869 \times 10^{-4}$	(+)	1.3773×10^{-11}
	SEDE	$\mathbf{1.72981370994070 \times 10^{-3}}$	$1.72981370994066 \times 10^{-3}$	$\mathbf{1.72981370994068 \times 10^{-3}}$	$1.24745772198282 \times 10^{-17}$	(+)	2.0390×10^{-2}
	DOLADE	$\mathbf{1.72981370994070 \times 10^{-3}}$	$1.72981370994066 \times 10^{-3}$	$\mathbf{1.72981370994068 \times 10^{-3}}$	$\mathbf{9.16570947960752 \times 10^{-18}}$	(+)	6.8532×10^{-3}
	IWOA	$1.89009612817313 \times 10^{-3}$	$1.73243299926313 \times 10^{-3}$	$1.80107707717986 \times 10^{-3}$	$3.34272034354920 \times 10^{-5}$	(+)	1.4295×10^{-11}
	PGJAYA	$1.74876658470105 \times 10^{-3}$	$1.72981397145254 \times 10^{-3}$	$1.73077791266686 \times 10^{-3}$	$3.45844480461756 \times 10^{-6}$	(+)	1.3531×10^{-11}
	IGSK	$\mathbf{1.72981370994070 \times 10^{-3}}$	$1.72981370994066 \times 10^{-3}$	$\mathbf{1.72981370994068 \times 10^{-3}}$	$1.43583193270945 \times 10^{-17}$	(+)	1.8744×10^{-2}
	LaPSO	$1.46802616521865 \times 10^{-1}$	$1.72981370994068 \times 10^{-3}$	$6.83425884513958 \times 10^{-3}$	$2.59981175065994 \times 10^{-2}$	(+)	3.3622×10^{-6}
	RTLBO	$2.03259457471086 \times 10^{-3}$	$1.72981674269726 \times 10^{-3}$	$1.75707325040703 \times 10^{-3}$	$5.52642113734253 \times 10^{-5}$	(+)	1.4295×10^{-11}
STP6-120/36	DODE	$1.66006031250855 \times 10^{-2}$	$\mathbf{1.66006031250846 \times 10^{-2}}$	$\mathbf{1.66006031250850 \times 10^{-2}}$	$2.04948114449183 \times 10^{-16}$	NA	NA
	JADE	$3.23869693230732 \times 10^{-2}$	$1.66006031304504 \times 10^{-2}$	$2.35124969859339 \times 10^{-2}$	$4.76162310942712 \times 10^{-3}$	(+)	1.5080×10^{-11}
	CoDE	$1.66006031250892 \times 10^{-2}$	$1.66006031250856 \times 10^{-2}$	$1.66006031250862 \times 10^{-2}$	$7.62895279964384 \times 10^{-16}$	(+)	1.5070×10^{-11}
	MPEDE	$1.82620932807556 \times 10^{-2}$	$1.66022624048459 \times 10^{-2}$	$1.69172833234824 \times 10^{-2}$	$4.21939732308916 \times 10^{-4}$	(+)	1.5080×10^{-11}
	SEDE	$1.66006031250856 \times 10^{-2}$	$1.66006031250850 \times 10^{-2}$	$1.66006031250853 \times 10^{-2}$	$1.56419096552865 \times 10^{-16}$	(+)	4.3699×10^{-7}
	DOLADE	$\mathbf{1.66006031250854 \times 10^{-2}}$	$1.66006031250848 \times 10^{-2}$	$1.66006031250852 \times 10^{-2}$	$1.53948604759203 \times 10^{-16}$	(+)	7.1962×10^{-4}
	IWOA	$1.79420615507602 \times 10^{-2}$	$1.66007104108898 \times 10^{-2}$	$1.70674957253113 \times 10^{-2}$	$3.73519403638798 \times 10^{-4}$	(+)	1.5080×10^{-11}
	PGJAYA	$1.67838656900354 \times 10^{-2}$	$1.66006033230863 \times 10^{-2}$	$1.66077600606031 \times 10^{-2}$	$3.27754428313028 \times 10^{-5}$	(+)	1.4957×10^{-11}
	IGSK	$1.66006031250856 \times 10^{-2}$	$1.66006031250849 \times 10^{-2}$	$1.66006031250853 \times 10^{-2}$	$\mathbf{1.46366533003527 \times 10^{-16}}$	(+)	9.2828×10^{-7}
	LaPSO	1.00180624317972	$1.66006031250853 \times 10^{-2}$	$5.90955682568764 \times 10^{-2}$	$1.82562599818994 \times 10^{-1}$	(+)	4.1546×10^{-11}
	RTLBO	$4.53742241915738 \times 10^{-2}$	$1.66006281589215 \times 10^{-2}$	$1.78173047683371 \times 10^{-2}$	$5.23759995710919 \times 10^{-3}$	(+)	1.5080×10^{-11}

(6) For the STP6-120/36 module model, DODE obtains the best Min and Mean compared to others. DOLADE obtains the best Max value, while IGSK possesses the best SD. From the statistical results, it is observed that DODE still maintains a competitive advantage compared to other algorithms.

As a further comparison, the Friedman test [80] is adopted to obtain the overall rankings of all 11 tested algorithms on the six PV problems. In the Friedman test, the null hypothesis postulates that the average values of all tested methods are equal. Then, all algorithms are ranked based on their average values across each problem, and the average ranking of each algorithm among all problems is calculated to evaluate their respective performance. A lower average ranking indicates that the corresponding algorithm performs better. The overall ranking results of all compared algorithms are illustrated in Figure 9. It is evident that the proposed DODE algorithm is the top-performing algorithm in comparison to all opponents by yielding the best average ranking of 1.67 for six PV models, followed by SEDE and DOLADE, with average rankings of 2.58 and 2.67, respectively.

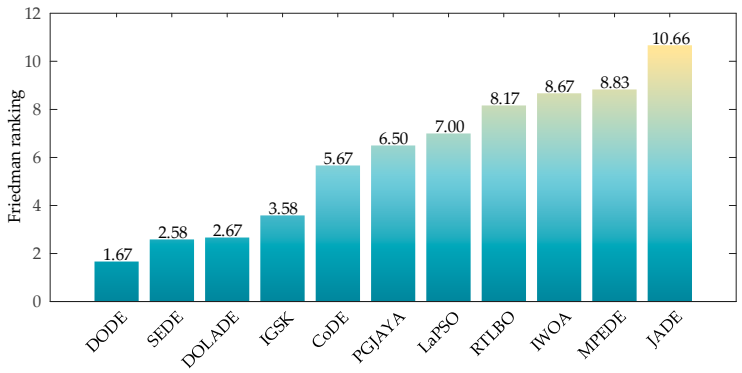

Figure 9. Friedman rankings of all 11 tested algorithms under a significance level α = 0.05 for the above six PV models.

Additionally, the computational cost of each tested algorithm on the above six PV models is illustrated in Figure 10. This shows that, despite the consistency in the maximum number of fitness evaluations, the total computation time varies among the algorithms due to differences in their computational complexity. Specifically, IGSK possesses the shortest computation cost, while RTLBO possesses the longest. The computational costs of the remaining algorithms are nearly equivalent, and the slight increase in the computation cost of DODE is acceptable.

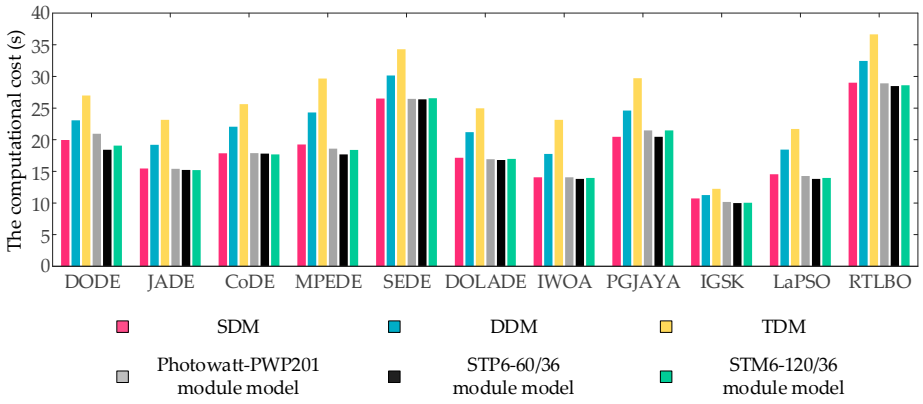

Figure 10. The computational time (s) of all 11 tested algorithms on six PV models.

6. Conclusions

To determine optimal parameters in the operation of PV systems, this paper develops an improved differential evolution algorithm, termed DODE, to accurately and efficiently extract some unknown parameters in various PV models. DODE innovatively integrates a novel collaboration mechanism of dual mutation strategies and an orientation guidance mechanism, effectively leveraging individual information at different stages and population evolution orientation to enhance the optimization capability of DE. The equivalent circuits are provided based on the diode, and the mathematical formulations of problems are constructed. The RMSE is utilized as one of the standards for evaluating the algorithmic quality. Extensive comparisons are made with existing state-of-the-art algorithms on PV model parameter identification, and the simulated data and measured data are presented. *I-V* and *P-V* characteristic curves are plotted. The convergence curves depict that DODE yields the optimal values of identified parameters, and the corresponding RMSE values are $9.86021877891317 \times 10^{-4}$, $9.82484851784979 \times 10^{-4}$, $9.82484851784993 \times 10^{-4}$, $2.42507486809489 \times 10^{-3}$, $1.72981370994064 \times 10^{-3}$, and $1.66006031250846 \times 10^{-2}$, 6.0600×10^{-4} for the six different PV modules. Further, the statistical analysis based on two non-parametric test methods (i.e., the Wilcoxon rank-sum and the Friedman tests), shows that the DODE algorithm effectively addresses these issues and achieves highly competitive experimental results.

To summarize, DODE shows a powerful performance compared with these advanced algorithms regarding the accuracy and reliability of identified parameters, the convergence characteristics, and some statistical indexes. However, a few constraints still need to be further considered in future work. Firstly, DODE should be applied to the parameter identification problem of other PV scenarios to thoroughly verify its optimization capabilities. In particular, its performance can be further demonstrated under different experimental conditions, such as variations in ambient temperature, irradiance, wind speed, shading condition, and other ever-changing and uncontrollable factors. Then, the feasibility and adaptability of DODE can be further improved by combining the design principles of other optimization algorithms. The authors believe that DODE cannot be considered a ubiquitous method because, according to the description of the "No Free Lunch" theorem, no one method can solve all optimization issues.

Author Contributions: Conceptualization, S.Y. and W.Z.; methodology, S.Y. and W.Z.; software, S.Y. and Y.J.; validation, Y.J., Y.C. and X.L.; formal analysis, S.Y., Y.J. and Y.C.; investigation, Y.J. and X.L.; resources, Y.J.; data curation, S.Y., Y.J. and Y.C.; writing—original draft preparation, S.Y.; writing—review and editing, W.Z.; visualization, S.Y. and Y.J.; supervision, W.Z.; project administration, W.Z.; funding acquisition, W.Z. All authors have read and agreed to the published version of the manuscript.

Funding: This study was supported by the National Key Research and Development Program of China [grant number 2017YFA0700300].

Institutional Review Board Statement: Not applicable.

Informed Consent Statement: Not applicable.

Data Availability Statement: Not applicable.

Conflicts of Interest: The authors declare no conflict of interest.

References

1. Haider, R.; D'Achiardi, D.; Venkataramanan, V.; Srivastava, A.; Bose, A.; Annaswamy, A.M. Reinventing the utility for distributed energy resources: A proposal for retail electricity markets. *Adv. Appl. Energy* **2021**, *2*, 100026. [CrossRef]
2. Yang, L.; Li, X.; Sun, M.; Sun, C. Hybrid policy-based reinforcement learning of adaptive energy management for the Energy transmission-constrained island group. *IEEE Trans. Ind. Inf.* **2023**. [CrossRef]
3. Zhang, N.; Sun, Q.; Yang, L.; Li, Y. Event-triggered distributed hybrid control scheme for the integrated energy system. *IEEE Trans. Ind. Inf.* **2021**, *18*, 835–846. [CrossRef]

4. Hossain, M.A.; Pota, H.R.; Hossain, M.J.; Blaabjerg, F. Evolution of microgrids with converter-interfaced generations: Challenges and opportunities. *Int. J. Electr. Power Energy Syst.* **2019**, *109*, 160–186. [CrossRef]
5. Zhang, Y.; Samuel, I.D.W.; Wang, T.; Lidzey, D.G. Current status of outdoor lifetime testing of organic photovoltaics. *Adv. Sci.* **2018**, *5*, 1800434. [CrossRef]
6. Priyadarshi, N.; Padmanaban, S.; Bhaskar, M.S.; Blaabjerg, F.; Holm-Nielsen, J.B.; Azam, F.; Sharma, A.K. A hybrid photovoltaic-fuel cell-based single-stage grid integration with Lyapunov control scheme. *IEEE Syst. J.* **2019**, *14*, 3334–3342. [CrossRef]
7. Elshahed, M.; El-Rifaie, A.M.; Tolba, M.A.; Ginidi, A.; Shaheen, A.; Mohamed, S.A. An Innovative Hunter-Prey-Based Optimization for Electrically Based Single-, Double-, and Triple-Diode Models of Solar Photovoltaic Systems. *Mathematics* **2022**, *10*, 4625. [CrossRef]
8. Jordehi, A.R. Enhanced leader particle swarm optimisation (ELPSO): An efficient algorithm for parameter estimation of photovoltaic (PV) cells and modules. *Sol. Energy* **2018**, *159*, 78–87. [CrossRef]
9. Aribia, H.B.; El-Rifaie, A.M.; Tolba, M.A.; Shaheen, A.; Moustafa, G.; Elsayed, F.; Elshahed, M. Growth Optimizer for Parameter Identification of Solar Photovoltaic Cells and Modules. *Sustainability* **2023**, *15*, 7896. [CrossRef]
10. Chin, V.J.; Salam, Z.; Ishaque, K. Cell modelling and model parameters estimation techniques for photovoltaic simulator application: A review. *Appl. Energy* **2015**, *154*, 500–519. [CrossRef]
11. Pillai, D.S.; Rajasekar, N. Metaheuristic algorithms for PV parameter identification: A comprehensive review with an application to threshold setting for fault detection in PV systems. *Renew. Sustain. Energy Rev.* **2018**, *82*, 3503–3525. [CrossRef]
12. Al-Shahri, O.A.; Ismail, F.B.; Hannan, M.A.; Lipu, M.S.H.; Al-Shetwi, A.Q.; Begum, R.A.; Al-Muhsen, N.F.O.; Soujeri, E. Solar photovoltaic energy optimization methods, challenges and issues: A comprehensive review. *J. Clean. Prod.* **2021**, *284*, 125465. [CrossRef]
13. Abbassi, R.; Abbassi, A.; Jemli, M.; Chebbi, S. Identification of unknown parameters of solar cell models: A comprehensive overview of available approaches. *Renew. Sustain. Energy Rev.* **2018**, *90*, 453–474. [CrossRef]
14. Farah, A.; Belazi, A.; Benabdallah, F.; Almalaq, A.; Chtourou, M.; Abido, M.A. Parameter extraction of photovoltaic models using a comprehensive learning Rao-1 algorithm. *Energy Convers. Manag.* **2022**, *252*, 115057. [CrossRef]
15. Choulli, I.; Elyaqouti, M.; Saadaoui, D.; Lidaighbi, S.; Elhammoudy, A.; Obukhov, S.; Ibrahim, A. A novel hybrid analytical/iterative method to extract the single-diode model's parameters using Lambert's W-function. *Energy Convers. Manag. X* **2023**, *18*, 100362. [CrossRef]
16. Premkumar, M.; Jangir, P.; Sowmya, R. Parameter extraction of three-diode solar photovoltaic model using a new metaheuristic resistance–capacitance optimization algorithm and improved Newton–Raphson method. *J. Comput. Electron.* **2023**, *22*, 439–470. [CrossRef]
17. Li, S.; Gu, Q.; Gong, W.; Ning, B. An enhanced adaptive differential evolution algorithm for parameter extraction of photovoltaic models. *Energy Convers. Manag.* **2020**, *205*, 112443. [CrossRef]
18. Yang, C.; Su, C.; Hu, H.; Habibi, M.; Safarpour, H.; Khadimallah, M.A. Performance optimization of photovoltaic and solar cells via a hybrid and efficient chimp algorithm. *Sol. Energy* **2023**, *253*, 343–359. [CrossRef]
19. Elaziz, M.A.; Thanikanti, S.B.; Ibrahim, I.A.; Lu, S.; Nastasi, B.; Alotaibi, M.A.; Hossain, M.A.; Yousri, D. Enhanced marine predators algorithm for identifying static and dynamic photovoltaic models parameters. *Energy Convers. Manag.* **2021**, *236*, 113971. [CrossRef]
20. Xiong, G.; Li, L.; Mohamed, A.W.; Yuan, X.; Zhang, J. A new method for parameter extraction of solar photovoltaic models using gaining–sharing knowledge based algorithm. *Energy Rep.* **2021**, *7*, 3286–3301. [CrossRef]
21. Gao, S.; Wang, K.; Tao, S.; Jin, T.; Dai, H.; Cheng, J. A state-of-the-art differential evolution algorithm for parameter estimation of solar photovoltaic models. *Energy Convers. Manag.* **2021**, *230*, 113784. [CrossRef]
22. Ishaque, K.; Salam, Z.; Mekhilef, S.; Shamsudin, A. Parameter extraction of solar photovoltaic modules using penalty-based differential evolution. *Appl. Energy* **2012**, *99*, 297–308. [CrossRef]
23. Ye, M.; Wang, X.; Xu, Y. Parameter extraction of solar cells using particle swarm optimization. *J. Appl. Phys.* **2009**, *105*, 094502. [CrossRef]
24. Fan, Y.; Wang, P.; Heidari, A.A.; Chen, H.; Mafarja, M. Random reselection particle swarm optimization for optimal design of solar photovoltaic modules. *Energy* **2022**, *239*, 121865. [CrossRef]
25. Sallam, K.M.; Hossain, M.A.; Chakrabortty, R.K.; Ryan, M.J. An improved gaining-sharing knowledge algorithm for parameter extraction of photovoltaic models. *Energy Convers. Manag.* **2021**, *237*, 114030. [CrossRef]
26. Oliva, D.; Abd El Aziz, M.; Hassanien, A.E. Parameter estimation of photovoltaic cells using an improved chaotic whale optimization algorithm. *Appl. Energy* **2017**, *200*, 141–154. [CrossRef]
27. Xiong, G.; Zhang, J.; Shi, D.; He, Y. Parameter extraction of solar photovoltaic models using an improved whale optimization algorithm. *Energy Convers. Manag.* **2018**, *174*, 388–405. [CrossRef]
28. Zagrouba, M.; Sellami, A.; Bouaïcha, M.; Ksouri, M. Identification of PV solar cells and modules parameters using the genetic algorithms: Application to maximum power extraction. *Sol. Energy* **2010**, *84*, 860–866. [CrossRef]
29. Chen, X.; Xu, B.; Mei, C.; Ding, Y.; Li, K. Teaching–learning–based artificial bee colony for solar photovoltaic parameter estimation. *Appl. Energy* **2018**, *212*, 1578–1588. [CrossRef]
30. Oliva, D.; Cuevas, E.; Pajares, G. Parameter identification of solar cells using artificial bee colony optimization. *Energy* **2014**, *72*, 93–102. [CrossRef]

31. Sharma, A.; Sharma, A.; Moshe, A.; Raj, N.; Pachauri, R.K. An effective method for parameter estimation of solar PV cell using Grey-wolf optimization technique. *Int. J. Math. Eng. Manag. Sci.* **2021**, *6*, 911. [CrossRef]
32. Yu, K.; Liang, J.J.; Qu, B.Y.; Chen, X.; Wang, H. Parameters identification of photovoltaic models using an improved JAYA optimization algorithm. *Energy Convers. Manag.* **2017**, *150*, 742–753. [CrossRef]
33. Premkumar, M.; Jangir, P.; Sowmya, R.; Elavarasan, R.M.; Kumar, B.S. Enhanced chaotic JAYA algorithm for parameter estimation of photovoltaic cell/modules. *ISA Trans.* **2021**, *116*, 139–166. [CrossRef] [PubMed]
34. Senthilkumar, S.; Mohan, V.; Krithiga, G. Brief review on solar photovoltaic parameter estimation of single and double diode model using evolutionary algorithms. *Int. J. Eng. Technol. Manag. Res.* **2023**, *10*, 64–78. [CrossRef]
35. Hassan, A.Y.; Ismaeel, A.A.K.; Said, M.; Ghoniem, R.M.; Deb, S.; Elsayed, A.G. Evaluation of Weighted Mean of Vectors Algorithm for Identification of Solar Cell Parameters. *Processes* **2022**, *10*, 1072. [CrossRef]
36. El-Sehiemy, R.; Shaheen, A.; El-Fergany, A.; Ginidi, A. Electrical parameters extraction of PV modules using artificial hummingbird optimizer. *Sci. Rep.* **2023**, *13*, 9240. [CrossRef] [PubMed]
37. Ginidi, A.R.; Shaheen, A.M.; El-Sehiemy, R.A.; Hasanien, H.M.; Al-Durra, A. Estimation of electrical parameters of photovoltaic panels using heap-based algorithm. *IET Renew. Power Gener.* **2022**, *16*, 2292–2312. [CrossRef]
38. Sharma, A.; Sharma, A.; Chowdary, V.; Srivastava, A.; Joshi, P. Cuckoo search algorithm: A review of recent variants and engineering applications. In *Metaheuristic and Evolutionary Computation: Algorithms and Applications*; Springer: Singapore, 2021; pp. 177–194.
39. Gu, Z.; Xiong, G.; Fu, X.; Mohamed, A.W.; Al-Betar, M.A.; Chen, H.; Chen, J. Extracting accurate parameters of photovoltaic cell models via elite learning adaptive differential evolution. *Energy Convers. Manag.* **2023**, *285*, 116994. [CrossRef]
40. Jordehi, A.R. Time varying acceleration coefficients particle swarm optimisation (TVACPSO): A new optimisation algorithm for estimating parameters of PV cells and modules. *Energy Convers. Manag.* **2016**, *129*, 262–274. [CrossRef]
41. Merchaoui, M.; Sakly, A.; Mimouni, M.F. Particle swarm optimisation with adaptive mutation strategy for photovoltaic solar cell/module parameter extraction. *Energy Convers. Manag.* **2018**, *175*, 151–163. [CrossRef]
42. Xiong, G.; Li, L.; Mohamed, A.W.; Zhang, J.; Zhang, Y.; Chen, H. Optimal identification of unknown parameters of photovoltaic models using dual-population gaining-sharing knowledge-based algorithm. *Int. J. Intell. Syst.* **2023**, *2023*, 3788453. [CrossRef]
43. Hamid, N.; Abounacer, R.; Idali Oumhand, M.; Feddaoui, M.; Agliz, D. Parameters identification of photovoltaic solar cells and module using the genetic algorithm with convex combination crossover. *Int. J. Ambient Energy* **2019**, *40*, 517–524. [CrossRef]
44. Saadaoui, D.; Elyaqouti, M.; Assalaou, K.; Lidaighbi, S. Parameters optimization of solar PV cell/module using genetic algorithm based on non-uniform mutation. *Energy Convers. Manag. X* **2021**, *12*, 100129. [CrossRef]
45. Oliva, D.; Ewees, A.A.; Aziz, M.A.E.; Hassanien, A.E.; Peréz-Cisneros, M. A Chaotic Improved Artificial Bee Colony for Parameter Estimation of Photovoltaic Cells. *Energies* **2017**, *10*, 865. [CrossRef]
46. Qu, C.; Lu, Z.; Peng, X.; Lin, G. A Hunter-Prey Algorithm Coordinating Mutual Benefit and Sharing and Interactive Learning for High-Efficiency Design of Photovoltaic Models. *Int. J. Intell. Syst.* **2023**, *2023*, 4831209. [CrossRef]
47. Sharma, A.; Sharma, A.; Averbukh, M.; Rajput, S.; Jately, V.; Choudhury, S.; Azzopardi, B. Improved moth flame optimization algorithm based on opposition-based learning and Lévy flight distribution for parameter estimation of solar module. *Energy Rep.* **2022**, *8*, 6576–6592. [CrossRef]
48. Sharma, A.; Sharma, A.; Averbukh, M.; Jately, V.; Rajput, S.; Azzopardi, B.; Lim, W.H. Performance investigation of state-of-the-art metaheuristic techniques for parameter extraction of solar cells/module. *Sci. Rep.* **2023**, *13*, 11134. [CrossRef]
49. Jordehi, A.R. Parameter estimation of solar photovoltaic (PV) cells: A review. *Renew. Sustain. Energy Rev.* **2016**, *61*, 354–371. [CrossRef]
50. Venkateswari, R.; Rajasekar, N. Review on parameter estimation techniques of solar photovoltaic systems. *Int. Trans. Electr. Energy Syst.* **2021**, *31*, e13113. [CrossRef]
51. Yang, X.; Gong, W.; Wang, L. Comparative study on parameter extraction of photovoltaic models via differential evolution. *Energy Convers. Manag.* **2019**, *201*, 112113. [CrossRef]
52. Liang, J.; Qiao, K.; Yu, K.; Ge, S.; Qu, B.; Xu, R.; Li, K. Parameters estimation of solar photovoltaic models via a self-adaptive ensemble-based differential evolution. *Sol. Energy* **2020**, *207*, 336–346. [CrossRef]
53. Zhou, J.; Zhang, Y.; Zhang, Y.; Shang, W.-L.; Yang, Z.; Feng, W. Parameters identification of photovoltaic models using a differential evolution algorithm based on elite and obsolete dynamic learning. *Appl. Energy* **2022**, *314*, 118877. [CrossRef]
54. Gude, S.; Jana, K.C. Parameter extraction of photovoltaic cell using an improved cuckoo search optimization. *Sol. Energy* **2020**, *204*, 280–293. [CrossRef]
55. Naeijian, M.; Rahimnejad, A.; Ebrahimi, S.M.; Pourmousa, N.; Gadsden, S.A. Parameter estimation of PV solar cells and modules using Whippy Harris Hawks Optimization Algorithm. *Energy Rep.* **2021**, *7*, 4047–4063. [CrossRef]
56. Askarzadeh, A.; Rezazadeh, A. Parameter identification for solar cell models using harmony search-based algorithms. *Sol. Energy* **2012**, *86*, 3241–3249. [CrossRef]
57. Yousri, D.; Thanikanti, S.B.; Allam, D.; Ramachandaramurthy, V.K.; Eteiba, M. Fractional chaotic ensemble particle swarm optimizer for identifying the single, double, and three diode photovoltaic models' parameters. *Energy* **2020**, *195*, 116979. [CrossRef]
58. Ibrahim, I.A.; Hossain, M.; Duck, B.C.; Nadarajah, M. An improved wind driven optimization algorithm for parameters identification of a triple-diode photovoltaic cell model. *Energy Convers. Manag.* **2020**, *213*, 112872. [CrossRef]

59. Yang, B.; Wang, J.; Zhang, X.; Yu, T.; Yao, W.; Shu, H.; Zeng, F.; Sun, L. Comprehensive overview of meta-heuristic algorithm applications on PV cell parameter identification. *Energy Convers. Manag.* **2020**, *208*, 112595. [CrossRef]
60. Shaheen, A.; El-Sehiemy, R.; El-Fergany, A.; Ginidi, A. Representations of solar photovoltaic triple-diode models using artificial hummingbird optimizer. *Energy Sources Part A* **2022**, *44*, 8787–8810. [CrossRef]
61. Yu, K.; Liang, J.J.; Qu, B.Y.; Cheng, Z.; Wang, H. Multiple learning backtracking search algorithm for estimating parameters of photovoltaic models. *Appl. Energy* **2018**, *226*, 408–422. [CrossRef]
62. Li, Y.; Yu, K.; Liang, J.; Yue, C.; Qiao, K. A landscape-aware particle swarm optimization for parameter identification of photovoltaic models. *Appl. Soft Comput.* **2022**, *131*, 109793. [CrossRef]
63. Goh, H.H.; Luo, Q.; Zhang, D.; Liu, H.; Dai, W.; Lim, C.S.; Kurniawan, T.A.; Goh, K.C. Hybrid SDS and WPT-IBBO-DNM Based Model for Ultra-short Term Photovoltaic Prediction. *CSEE J. Power Energy Syst.* **2022**, *9*, 66–76.
64. Zhang, J.; Sanderson, A.C. JADE: Adaptive differential evolution with optional external archive. *IEEE Trans. Evol. Comput.* **2009**, *13*, 945–958. [CrossRef]
65. Bayraktar, Z.; Komurcu, M.; Bossard, J.A.; Werner, D.H. The wind driven optimization technique and its application in electromagnetics. *IEEE Trans. Antennas Propag.* **2013**, *61*, 2745–2757. [CrossRef]
66. Wu, G.; Mallipeddi, R.; Suganthan, P.N. Ensemble strategies for population-based optimization algorithms—A survey. *Swarm Evol. Comput.* **2019**, *44*, 695–711. [CrossRef]
67. Gui, L.; Xia, X.; Yu, F.; Wu, H.; Wu, R.; Wei, B.; Zhang, Y.; Li, X.; He, G. A multi-role based differential evolution. *Swarm Evol. Comput.* **2019**, *50*, 100508. [CrossRef]
68. Wu, G.; Mallipeddi, R.; Suganthan, P.N.; Wang, R.; Chen, H. Differential evolution with multi-population based ensemble of mutation strategies. *Inf. Sci.* **2016**, *329*, 329–345. [CrossRef]
69. Price, K.; Storn, R.M.; Lampinen, J.A. *Differential Evolution: A Practical Approach to Global Optimization*; Springer Science & Business Media: Berlin/Heidelberg, Germany, 2006.
70. Biedrzycki, R. Handling bound constraints in CMA-ES: An experimental study. *Swarm Evol. Comput.* **2020**, *52*, 100627. [CrossRef]
71. Storn, R.; Price, K. Differential evolution–a simple and efficient heuristic for global optimization over continuous spaces. *J. Glob. Optim.* **1997**, *11*, 341–359. [CrossRef]
72. Wang, Y.; Cai, Z.; Zhang, Q. Differential evolution with composite trial vector generation strategies and control parameters. *IEEE Trans. Evol. Comput.* **2011**, *15*, 55–66. [CrossRef]
73. Easwarakhanthan, T.; Bottin, J.; Bouhouch, I.; Boutrit, C. Nonlinear minimization algorithm for determining the solar cell parameters with microcomputers. *J. Sol. Energy* **1986**, *4*, 1–12. [CrossRef]
74. Tong, N.T.; Pora, W. A parameter extraction technique exploiting intrinsic properties of solar cells. *Appl. Energy* **2016**, *176*, 104–115. [CrossRef]
75. Gao, X.; Cui, Y.; Hu, J.; Xu, G.; Wang, Z.; Qu, J.; Wang, H. Parameter extraction of solar cell models using improved shuffled complex evolution algorithm. *Energy Convers. Manag.* **2018**, *157*, 460–479. [CrossRef]
76. Yu, K.; Qu, B.; Yue, C.; Ge, S.; Chen, X.; Liang, J. A performance-guided JAYA algorithm for parameters identification of photovoltaic cell and module. *Appl. Energy* **2019**, *237*, 241–257. [CrossRef]
77. Yu, X.; Hu, Z.; Wang, X.; Luo, W. Ranking teaching–learning-based optimization algorithm to estimate the parameters of solar models. *Eng. Appl. Artif. Intell.* **2023**, *123*, 106225. [CrossRef]
78. Huang, C.; Li, Y.; Yao, X. A survey of automatic parameter tuning methods for metaheuristics. *IEEE Trans. Evol. Comput.* **2019**, *24*, 201–216. [CrossRef]
79. Carrasco, J.; García, S.; Rueda, M.M.; Das, S.; Herrera, F. Recent trends in the use of statistical tests for comparing swarm and evolutionary computing algorithms: Practical guidelines and a critical review. *Swarm Evol. Comput.* **2020**, *54*, 100665. [CrossRef]
80. Zimmerman, D.W.; Zumbo, B.D. Relative power of the Wilcoxon test, the Friedman test, and repeated-measures ANOVA on ranks. *J. Exp. Educ.* **1993**, *62*, 75–86. [CrossRef]